ORIGINAL RESEARCH

Synthesis of Zinc Oxide-Doped Carbon Dots for Treatment of Triple-Negative Breast Cancer

Mengqi Wang [1],*, Shuting Lan [2],*, Mingjun Song[3], Rongrong Zhang [2], Wenqi Zhang [2], Xiaomei Sun [2], Gang Liu [2]

[1]College of Life Science and Oceanography, Weifang University, Weifang, Shandong, People's Republic of China; [2]Key Laboratory of Medical Cell Biology, Affiliated Hospital of Inner Mongolia Medical University, Hohhot, Inner Mongolia, People's Republic of China; [3]College of Chemical Engineering and Environmental Chemistry, Weifang University, Weifang, Shandong, People's Republic of China

*These authors contributed equally to this work

Correspondence: Mengqi Wang; Gang Liu, Email wangmengqi@tju.edu.cn; 20190043@immu.edu.cn

Introduction: The anti-cancer properties of zinc oxide-doped carbon dots (CDs/ZnO) in inhibiting triple-negative breast cancer (TNBC) progression merit more investigation.

Methods: With citric acid as the carbon source, urea applied as the nitrogen source, and zinc oxide (ZnO) used as a reactive dopant, CDs/ZnO were synthesized by microwave heating in the current study, followed by the characterization and biocompatibility assessments. Subsequently, the anti-cancer capabilities of CDs/ZnO against TNBC progression were evaluated by various biochemical and molecular techniques, including viability, proliferation, migration, invasion, adhesion, clonogenicity, cell cycle distribution, apoptosis, redox homeostasis, metabolome, and transcriptome assays of MDA-MB-231 cells. Additionally, the in vivo anti-cancer potentials of CDs/ZnO against TNBC progression were analyzed using TNBC xenograft mouse models.

Results: The biocompatibility of CDs/ZnO was supported by the non-significant changes in the pathological and physiological parameters in the CDs/ZnO treated mice, alongside a non-cytotoxic effect of CDs/ZnO on the proliferation of normal cells. Notably, the CDs/ZnO treatments effectively decreased the viability, proliferation, migration, invasion, adhesion, and clonogenicity of MDA-MB-231 cells. Furthermore, the CDs/ZnO treatments induced cell cycle arrest, apoptosis, redox imbalance, metabolome disturbances, and transcriptomic alterations of MDA-MB-231 cells by regulating the MAPK signaling pathway. Additionally, the CDs/ZnO treatments markedly suppressed the in vivo tumor growth in the TNBC xenograft mouse models.

Conclusion: In this study, we synthesized CDs/ZnO via microwave heating, using citric acid as the carbon source, urea as the nitrogen source, and ZnO as a reactive dopant. We confirmed the biosafety and potent anti-cancer efficacy of CDs/ZnO in inhibiting TNBC progression by disrupting malignant cell behaviors through modulation of the MAPK signaling pathway.

Keywords: zinc, carbon dots, triple-negative breast cancer, MAPK signaling pathway

Introduction

As a consequence of population growth and aging, the future incidence of breast cancer is projected to increase by 40% to over 3 million newly diagnosed cases and 1 million estimated deaths annually by 2040, leading to the recent launch of the Global Breast Cancer Initiative by the World Health Organization (WHO) in 2021.[1] Incorporation of oncogenic driver mutations, various non-genetic risk events (such as hereditary, high mammographic density, chest radiation, high body mass index, menopausal hormone abuse, alcohol consumption, and inadequate physical activities) are contributing to the rising rates of breast cancer.[2,3] Although the survival rates of breast cancer patients have been improved by population-based breast cancer screening programs and timely diagnostic alternatives, along with adequate implementations of multidisciplinary precision preventives and individualised cancer medications, the absolute disease burdens caused by local recurrences and invasive relapses remain high among women aged 30 to 60 globally.[4]

13949

As an aggressive breast cancer subtype, triple-negative breast cancers (TNBC), coined in the mid-2000s and characterized by the expression absence of estrogen receptor (ER), progesterone receptor (PR), and human epidermal growth factor receptor 2 (HER2), accounts for approximately 15% to 20% of breast carcinomas.[5,6] As an umbrella term covering a heterogeneous variety of entities with marked genetic, transcriptional, immunomodulatory, histological, and clinical diversities, TNBC comprises a panoply of aggressive clinical behaviors and vastly different responses to clinical therapies.[7] Specifically, for these TNBC patients in the advanced-disease, the outcome remains disproportionately poor with a median survival of less than 24 months, on the other hand, the median survival time for metastatic TNBC patients is only 10.2 months to 13.3 months.[8]

Due to the lack of therapeutic targets, coupled with the absence of actionable biomarkers and molecular carcinoma drivers, the treatments of TNBC have been mainly based on chemotherapy as the standard of care. Of note, these neoadjuvant therapies, such as molecular-based precise therapies and immunotherapeutic interventions, have promisingly emerged as new therapeutical approaches for modest improvements in the prognosis of metastatic TNBC patients.[9] Nevertheless, less than 30% TNBC patients with achieve a complete response, and the acquired therapeutic resistance, recurrence, and mortality rates remain higher in these TNBC patients.[10] Hence, forthcoming research is warranted to benefit the therapeutic dependencies of TNBC better.

Since the discovery of nanodiamonds in the 1980s, functionalized nanocarbon materials with different dimensions have garnered multidisciplinary interest in applications ranging from electronics, photovoltaics, and optoelectronics to sensing, targeted bioimaging, drug delivery, diagnostics, and personalized therapeutics owing to their superior physical, chemical, optical, and electrocatalytic properties.[11,12] Driven by their unique structure-based chemical, electrical, and mechanical properties, nanocarbon materials have been employed as scaffolds for biological analytes of interest during clinical healthcare applications.[13] More importantly, these nanocarbon-based theranostics and diagnostics for cancer are emerging as noteworthy alternatives to clinical translations due to their qualities such as low intrinsic toxicity, peculiar biodistribution, low cost for large-scale production, and versatile surface functionalization.[14]

More specifically, carbon-based quantum dots (CQDs), including carbon dots (CDs), carbonized polymer dots (PDs), and graphene quantum dots (GQDs), have aroused the great interest of researchers since their discovery in 2004.[15] The highly desirable properties of CQDs, including biocompatibility, stability, controllable photoluminescence property, definite chemical structures, easily modified chemical structure, and catalytic performance, promote the promising application of CQDs in the field of tumor diagnosis and therapy strategies.[12,16] As the most widely researched type of CQDs, CDs have been proven as zero-dimensional carbon-based nanomaterials with extraordinary physicochemical properties and versatile applications.[16] Compared with the other nanocarbon materials, CDs have illustrated advantages in the structure and properties for their application in nanotheranostic strategies.[16] In addition, the flexible surface chemistry of CDs benefits the surface modification with other heteroatom, nanomaterials, and trace elements, enhancing the optical and electronic properties of CDs and providing additional characteristics of CDs to achieve precise cancer therapy.[17,18]

Recently, a wide range of zinc oxide-doped CDs (CDs/ZnO) with highly varying functionalities, including anti-cancer, antioxidant, anti-bacterial, anti-diabetic, anti-fungal, electrochemical, and photo-electrochemical sensing, have been effectively synthesized by using cost-effective and nontoxic green chemistry approaches.[19–21] However, the regulatory mechanism related to the anti-cancer potency of CDs/ZnO in interfacing with TNBC progression has not been investigated to date. In the current study, we developed a simple, rapid, efficient, and environmentally friendly synthesis method for CDs/ZnO, with the characterization and biocompatibility of CDs/ZnO further characterized by TEM, XPS, in vitro cell culture model, and in vivo mouse model. In addition, the TNBC cell culture model and TNBC xenograft mouse models were applied to confirm the inhibitory effect of CDs/ZnO treatments on TNBC progression, providing a fundamental basis for the clinical applications of CDs/ZnO.

Materials and Methods
Chemicals

Unless otherwise specified, the chemicals and supplementations utilized in the current study were procured from Sigma-Aldrich (Shanghai, China) and Thermo Fisher (Shanghai, China).

Synthesis and Characterization of CDs/ZnO

Following our previous work with minor modifications,[22] 3.0 g citric acid (C77920, Heowns, Tianjin, China) and 3.0 g urea (U111897, Aladdin, Shanghai, China) were blended with varying amounts of ZnO (1.2 g, 1.4 g, 1.6 g, 1.8 g, or 2.0 g, Z19221, Heowns, Tianjin, China), dissolved in 15.0 mL of H_2O, and subjected to microwave heating (750 W, Midea, China) for 10 min until the formation of yellow, foamy, and solid products. The upper layer of the substances was ground in an agate mortar and allowed to cool to room temperature.

For the characterization of CDs/ZnO, Transmission electron microscopy (TEM) images were obtained using the JEOL JEM-2100F Field Transmission Electron Microscope. X-ray diffraction (XRD) patterns were recorded by a Bruker D8 Focus Diffraction System with Cu Ka radiation (λ= 0.15406 nm). X-ray Photoelectron Spectroscopy (XPS) data were collected from the Thermo Fisher Escalab 250Xi using Al monochromatic Ka radiation (hv = 1486.6 eV) with spot size 500 μm as the X-ray source. The binding energies were referenced to the C 1s line at 284.8 eV from adventitious carbon. UV spectra of the CDs/ZnO in water were surveyed by the OCEAN OPTICS, DH-2000-BAL. Photoluminescence (PL) of both solid powder and the aqueous solution of CDs/ZnO was measured by an F-380 spectrophotometer, with the exit and entrance slit set as 5 nm. The time-resolved photoluminescence (TRPL) spectra were recorded by a nanosecond transient absorption emission spectrometer (NTAS) with an excitation wavelength λ=355 nm.

In vitro Biocompatibility Evaluation of CDs/ZnO

For in vitro biocompatibility evaluation of CDs/ZnO, a normal human gastric epithelial cell line (GES-1), a normal human ovarian granulosa line (KGN), and a normal human breast epithelial cell line (MCF 10A), were applied. KGN (CL-0603) and MCF 10A (CL-0525) cells, validated by the short tandem repeat profiling, were obtained from the Procell Life Science & Technology Co. Ltd., and cultured by their respective commercial culture medium (CM-0603 for KGN cells and CM-0525 for MCF 10A cells, Procell, Wuhan, China). GES-1 cells were kindly gifted by Mrs. Hua Du from the College of Life Science at Inner Mongolia University and cultured in a commercial culture medium (CM-0563, Procel, Wuhan, China).

For the CDs/ZnO treatments, the culture medium of GES-1, KGN, and MCF 10A cells was supplemented with varying concentrations of CDs/ZnO (20, 40, 80, and 160 μg/mL), and the cells were incubated for an additional 24 h, 48 h, and 72 h.[23] In addition, the GES-1, KGN, and MCF 10A cell cultured with the same volume of corresponding culture medium were set as the negative control (NC) group. Lastly, the viabilities of each group were detected at 24 h, 48 h, and 72 h post-treatment by a Countess II Automated Cell Counter.[24]

In vivo Biocompatibility Evaluation of CDs/ZnO

Twelve male Balb/c mice (6 weeks old) were used for the in vivo biocompatibility evaluation of CDs/ZnO and were housed under humanely controlled conditions. Standard balanced rodent diets were provided and consumed ad libitum. All animal-related experiments have been approved by the ethical standards of the Ethics Committee of Weifang University and conducted in compliance with national guidelines for animal welfare.

For the in vivo biocompatibility evaluation, six Balb/c mice were orally administered 50 mg/kg body weight of CDs/ZnO with the experimental group set as the CDs/ZnO group.[25] As the NC group, six Balb/c mice were orally administered an equal volume of saline solution. After daily treatments over 14 days, mice of both groups were weighed and the blood sample of both groups was collected with the renal/liver functions analyzed by assessing the plasma levels of alanine aminotransferase (ALT), aspartate aminotransferase (AST), blood urea nitrogen (BUN), and creatinine (CRE) by an automated chemistry analyzer. In addition, the blood levels of triglyceride (TG) and total cholesterol (TC) in both groups were detected by commercial kits (A110-1-1 for TG, A111-1-1 for TC, Jiancheng, Nanjing, China).

Afterward, all mice were sacrificed by cervical dislocation, and the liver, kidney, and spleen tissues of both groups were harvested and preserved in neutral buffered formalin solution (G2161, Solarbio, Beijing, China) overnight. After the preparation of paraffin sections,[26] the histological staining, including Hematoxylin and eosin (H&E) staining, Masson trichrome staining, and Periodic acid Schiff (PAS) staining, was performed to verify the in vivo biocompatibility of CDs/ZnO.

Cytotoxicity Effect Assay of CDs/ZnO Treatment Against TNBC Progression

After thawing, a human TNBC cell line, MDA-MB-231 cells were cultured at 37°C with 5% CO_2 in a humidified atmosphere by the culture medium of RPMI 1640 medium (01–100-1ACS, Biological Industries, Shanghai, China) supplemented with 10% fetal bovine serum (FBS, C04001, VivaCell, Shanghai, China) and 100 units/mL of penicillin-streptomycin antibiotics (P/S, 15070063, Thermo Fisher, Beijing, China).

Subsequently, the cytotoxicity effect of CDs/ZnO treatment against TNBC progression was analyzed by a 3-(4,5-dimethylthiazol-2-yl)-2,5-diphenyl tetrazolium bromide (MTT) assay. Briefly, MDA-MB-231 cells in the logarithmic growth phase were seeded in 96 wells-culture plates at a density of 5000 per well and cultured for an additional 24 h. For the CDs/ZnO treatments, the culture medium of MDA-MB-231 cells was individually supplemented with varying concentrations of CDs/ZnO (20, 40, 80, and 160 μg/mL) with the MDA-MB-231 cells then incubated for another 24 h. In addition, MDA-MB-231 cells cultured by the culture medium supplemented with an equal volume of Dulbecco's phosphate-buffered saline (DPBS, 14190250, Thermo Fisher, Beijing, China) were set as the NC group. After drug treatments for 24 h, the MDA-MB-231 cells of both groups were incubated with 10 μL of MTT solution (5 mg/mL, C0009S, Beyotime, Shanghai, China) for 2 h. After the supplementation of 100 μL of dimethyl sulfoxide solution (DMSO, CD4731, Coolaber, Beijing, China) to dissolve the purple crystal, the MDA-MB-231 cells of both groups were incubated for an additional 2 h with the absorbance values at 570 nm measured by a microtiter plate reader. Subsequently, the inhibiting rate (IR) of CDs/ZnO (20, 40, 80, and 160 μg/mL) treatment for 24 h on the viability of MDA-MB-231 cells was analyzed with the CDs/ZnO concentration applied for the following assessments optimized.

Wound-Healing Assay

As previously reported, the potential effect of CDs/ZnO treatment on the migration capacity of TNBC cells was confirmed by a wound-healing assay.[24] For the assay, MDA-MB-231 cells were collected, re-plated in 6-well culture plates, and cultured overnight. A wound across the cell monolayer was prepared by scratching the bottom of the 6-well culture plate with a 200 μL plastic pipette, and the serum-free cell culture medium of MDA-MB-231 cells was supplemented with either CDs/ZnO or DPBS solution. After a subsequent culture for 24 h, the wound closure of both groups was microscopically imaged.

Invasion Assay

The potential effect of CDs/ZnO treatment on the invasion ability of TNBC cells was characterized by a Transwell invasion assay. Accordingly, 2×10^3 MDA-MB-231 cells, suspended in the 200 μL of serum-free culture medium containing either CDs/ZnO or DPBS solution, were re-plated into the upper Transwell chamber, while 600 μL of culture medium was added to the lower compartment of the chamber, and the cells of both groups were cultured for 24 h. After carefully removing the non-migrating MDA-MB-231 cells in the upper Transwell chamber with a swab, the lower chambers were fixed in methanol, stained with 0.1% crystal violet solution (C0121, Beyotime, Shanghai, China) for 15 min, and then microscopically examined.[24]

Clonogenicity Assay

A clonogenicity assay was conducted to evaluate the effect of CDs/ZnO treatment against TNBC progression. Briefly, 1×10^3 MDA-MB-231 cells were collected, resuspended, re-plated in a 6-well culture plate, and cultured with the culture medium supplemented with either CDs/ZnO or DPBS solution. The cells of both groups were cultured for 7 d with the fresh culture medium changed daily. After fixation with 4% paraformaldehyde solution (P1110, Solarbio, Beijing, China), the colonies of both groups were stained with 0.1% crystal violet solution, and the detailed colonies number of both groups were microscopically examined.

Adhesion Assay

According to the departmental protocols, an adhesion assay was conducted to explore the potential effect of CDs/ZnO treatment against TNBC progression via inhibiting the adhesion potential of breast cancer cells. A total of 5×10^3 MDA-MB-231 cells treated by either CDs/ZnO or DPBS solution were collected, resuspended, and replated on fibronectin-

coated 96-well culture plates. After culturing at 37 °C for 30 min, the plates were gently washed with DPBS solution to remove non-adherent cells. The attached cells were then fixed with methanol and stained with 0.1% crystal violet solution. The detailed number of adherent cells in both groups was microscopically photographed and recorded.[24]

Cell Cycle Assay

For the cell cycle assay, MDA-MB-231 cells of both groups were collected, resuspended, and fixed with ice-cold 70% ethanol at −20 °C overnight. Following the instructions provided by the manufacturer, the MDA-MB-231 cells of both groups were stained by a cell cycle detection kit (CA1510, Solarbio, Beijing, China) with the cell cycle of each group analyzed via flow cytometry (FACS).[24]

Apoptosis Assay

For apoptosis assay, MDA-MB-231 cells treated with either CDs/ZnO or DPBS solution were collected, washed with pre-chilled (4 °C) DPBS solution, and incubated with the FITC conjugated Annexin V solution (CA1020, Solarbio, Beijing, China) at 37 °C for 5 min. After incubation of propidium iodide (PI) solution, FACS analysis was conducted within 1 h.

Redox Homeostasis Assessment

The effect of CDs/ZnO treatment on the redox homeostasis of MDA-MB-231 cells was confirmed by assessing ROS production, mitochondrial dysfunctions, and antioxidant enzyme activities.[24]

For assessing ROS production, MDA-MB-231 cells treated with either CDs/ZnO or DPBS solution were incubated with 10 μM dichlorofluorescein diacetate (DCFH-DA) solution (S0033, Beyotime, Shanghai, China) at 37 °C for 30 min. Following DAPI (C0065, Solarbio, Beijing, China) counterstaining, the DCFH-DA staining of each group was examined and recorded with the ROS production levels analyzed by the quantification of DCFH-DA staining intensity by Image J software.

For assessing the mitochondrial dysfunctions, MitoTracker staining, and JC-1 staining were employed. For MitoTracker staining, MDA-MB-231 cells treated with either CDs/ZnO or DPBS solution were washed with DPBS solution and incubated with 200 nM MitoTracker staining solution (C1049, Beyotime, Shanghai, China) at 37 °C for 30 min. After DAPI counterstaining, the MitoTracker staining was recorded with the MitoTracker staining intensity analyzed by Image J software. For JC-1 staining, MDA-MB-231 cells treated with either CDs/ZnO or DPBS solution were washed with DPBS solution and incubated with 10 μM JC-1 staining solution (C2006, Beyotime, Shanghai, China) at 37 °C for 20 min. Subsequently, the staining signals of J-aggregate (green staining intensity) and J-monomer (red staining intensity) were recorded with the mitochondrial membrane potential (ΔΨm) of each group analyzed by Image J software.

Additionally, the assessment of SOD, GSH, CAT, ATP, MDA, and LDH activities or levels was applied by commercial kits (S0109 for SOD, S0052 for GSH, S0051 for CAT, S0026 for ATP, S0131 for MDA, and C0018S for LDH, Beyotime, Shanghai, China) to determine the effects of CDs/ZnO treatments on triggering the redox imbalance of MDA-MB-231 cells.

Metabolomics Analysis

For metabolomics analysis, MDA-MB-231 cells treated with either CDs/ZnO or DPBS solution were washed with pre-chilled (4 °C) DPBS solution, collected via scraping, and immediately flash-frozen in liquid nitrogen. Afterward, the metabolite extraction was conducted by standard procedures with a quadrupole time-of-flight mass spectrometer coupled to hydrophilic interaction chromatography in Applied Protein Technology Co., Ltd (Shanghai, China).

After peak alignment, peak picking, and quantification, the raw data files were processed using Compound Discoverer 3.1 software. Subsequently, the peak intensities were normalized to the total spectral intensity, allowing the prediction of molecular formula according to the results of additive ions, molecular ion peaks, and fragment ions. Then the identified peaks were matched with the mzCloud, mzVault, and MassList databases to achieve accurate qualitative and relative quantitative results. Differential metabolites between the CDs/ZnO and NC groups were identified based on the following

criteria: variable importance in projection ≥1, |log2 fold change|≥1, and p<0.05. Kyoto Genes and Genomes (KEGG) enrichment analyses were performed using Fisher's exact test to explore the potential impact of differential metabolites. Only pathways with p<0.05 were considered as significantly changed pathways.

Transcriptomics Analysis

To elucidate the comprehensive regulatory mechanism underlying the effect of CDs/ZnO treatments against TNBC progression, RNA-Seq analysis of MDA-MB-231 cells treated with either CDs/ZnO or DPBS solution was performed by the Frasergen Biotechnology Company (Wuhan, China).[24,26]

Accordingly, the total mRNA of MDA-MB-231 cells treated with either CDs/ZnO or DPBS solution was extracted by Trizol reagents (Invitrogen, Carlsbad, CA, USA). The quality of mRNA was evaluated and checked by RNase-free agarose gel electrophoresis. Subsequently, the mRNA was enriched by Oligo (dT) beads, fragmented into short fragments by fragmentation buffer, and reverse transcribed into cDNA. The resulting double-stranded cDNA fragments from both groups were end-repaired, A base added, and ligated to the Illumina sequencing adapter. After purification of the ligation reaction, PCR amplification was conducted with the cDNA library sequenced using the Illumina Novaseq 6000 platform.

The raw RNA-Seq data was filtered for the bioinformatics analyses with the low-quality reads trimmed by the fastp software (Version 0.18.0). The clean reads were aligned to the reference genomic sequence with the transcript expression calculated by the RSEM software and the differentially expressed genes (DEGs) analyzed by the DESeq2 software. The genes with the parameter of false discovery rate (FDR)<0.05 and absolute fold change (FC) ≥ 2 were considered DEGs. All DEGs were then analyzed by gene ontology (GO) analysis and KEGG enrichment analysis.[27]

Western Blot

Western blot was utilized to determine the effect of CDs/ZnO treatment on disturbing the expression levels of epithelial-mesenchymal transition (EMT) and apoptosis-related proteins.[28] Moreover, the metabolomics and transcriptomic results of the significantly enriched signaling pathways in the MDA-MB-231 cells treated with either CDs/ZnO or DPBS solution were also validated by Western blot.

Total proteins from the MDA-MB-231 cells treated with either CDs/ZnO or DPBS solution were extracted by a RIPA lysis buffer (DE101, Transgen, Beijing, China), incubated at 90 °C for 5 min, and then centrifuged at 12,000 × g for 20 min. After quantification by a BCA assay kit (PC0020, Solarbio, Beijing, China), equal amounts of proteins (35 μg) from both groups were resolved on sodium dodecyl sulfate-polyacrylamide gel (SDS-PAGE) gels by a commercial kit (P1200, Solarbio, Beijing, China) and transferred to the polyvinylidene fluoride membranes (PVDF, PVH00010, Millipore, Beijing, China) with 1×Tris-glycine buffer (G2145, Servicebio, Wuhan, China). After rinsing the membranes with Tris-HCl solution supplemented with 0.1% Tween-20 (TBST) for triplicate, the PVDF membrane was incubated with the 10% non-fat milk solution for 1 h, and incubated with the various primary antibodies at 4 °C overnight. After rinsing 3 times with TBST, these membranes were incubated with the secondary antibodies at room temperature for 1 h. Lastly, the immunoblotted bands were visualized with the enhanced chemiluminescence solution (ECL, W1001, Promega, Beijing, China) in the ChampChemi system. The antibodies utilized in this study are listed in Supplementary Table 1.

In vivo Anti-Cancer Efficacy Assessment

For in vivo anti-tumor efficacy assessment, 5×10^5 4T1 cells were suspended in a volume of 100 μL of DPBS solution and subcutaneously injected into the right fourth mammary gland fat pad of the female Balb/c mice (6 weeks old) using a 0.5 mL insulin syringe. Once the tumor volume reached approximately 100 mm³, the Balb/c mice were randomly divided into two experimental groups: NC and CDs/ZnO. Every two days, six mice received subcutaneous injections of 50 mg/kg body weight of CDs/ZnO with the experimental group set as the CDs/ZnO group,[25] and the NC group was subcutaneously injected with the same volume of normal saline. All mice were sacrificed on day 15, and the tumors of both groups were collected, weighed, and measured with the tumor volume calculated as tumor = (length × width²)/2.

Histopathological Analysis of Xenograft Tissues

After fixation and the preparation of paraffin sections, the immunohistochemistry (IHC) staining and Terminal Deoxynucleotidyl Transferase dUTP Nick End Labelling (Tunel) staining of xenograft tissues were employed to assess the in vivo anti-cancer efficacy of CDs/ZnO against the TNBC progression.[29]

After dewaxing, rehydration, and antigen retrieval, the paraffin-embedded sections of each group, were incubated with 10% bovine albumin solution (BSA, SW3015, Solarbio, Beijing, China) at room temperature for 30 min. Subsequently, the sections were incubated with the primary antibodies at 4 °C overnight. Following this, the sections were washed with PBS solution and incubated with the corresponding HRP-labeled secondary antibodies at 25 °C for 30 min. After the incubation with the 3.3′-diaminobenzidine tetrahydrochloride (DAB) solution (DA1010, Solarbio, Beijing, China) at room temperature for 1 min, the immunostained sections were re-stained with hematoxylin solution for 3 min, sealed with neutral balsam (G8590, Solarbio, Beijing, China), and examined under a light microscope. Lastly, the positive staining intensities of each group were quantified and calculated by ImageJ software. The antibodies utilized in this study are listed in Supplementary Table 1.

For Tunel staining, the paraffin-embedded sections of each group were prepared. After deparaffinization and rehydration, the paraffin-embedded sections were washed with PBS solution and incubated with 20 μg/mL of Proteinase K solution (40306ES60, YEASAN, Shanghai, China) at room temperature for 5 min. Following a 30-minute incubation with equilibration buffer at room temperature, the sections were incubated with Terminal Deoxynucleotidyl Transferase (TdT) reaction solution at 37 °C for 60 min, followed by the incubation of TMR-5-dUTP Labeling Mix/TdT enzyme buffer (G1502, Servicebio, Wuhan, China) at room temperature for 30 min. Subsequently, the sections were incubated with the DAPI staining solution for 7 min. After section sealing and morphometric analyses of Tunel positive signals in each group, the apoptosis rates of each group were calculated by Image J software.

Statistical Analysis

In the present study, all data are presented as mean ± standard deviation (SD). For all tests, P values less than 0.05 were considered statistically significant. All statistical analyses were conducted by the Statistical Package for the Social Sciences software (SPSS, IBM, Version 19.0).

Results

Characteristics of CDs/ZnO

As shown in Supplementary Figure 1A, the synthesized CDs/ZnO exhibited yellow, foam, and solid appearances. When evaluating the fluorescence intensities of CDs/ZnO under 355 nm ultraviolet light, it was observed that the luminescence signals in the 1.2 g and 1.4 g ZnO-doped groups were weaker compared to those in the 1.6 g, 1.8 g, and 2.0 g ZnO-doped groups (Supplementary Figure 1B). Consequently, the 1.2 g and 1.4 g ZnO-doped groups were excluded from subsequent assays.

Figure 1A illustrates the XPS results for the 1.6 g, 1.8 g, and 2.0 g ZnO-doped groups, which exhibited similar spectral characteristics. Notably, the peak position and intensity of Zn-2p in those groups were nearly indistinguishable (Figure 1B), which closely aligned with our previous finding.[22] As shown in Table 1, the highest zinc content (5.16%) and oxygen content (39.25%) were detected in the 1.6 g ZnO-doped group, surpassing the levels found in the 1.8 g and 2.0 g ZnO-doped groups. Furthermore, the nitrogen content in the 1.6 g ZnO-doped group (29.26%) was higher than that in the 1.8 g ZnO-doped group, indicating a greater presence of active groups on the surface of CDs/ZnO.

As described in Supplementary Figure 2, the PL emission spectra of CDs/ZnO displayed similar shapes across all groups, with a distinct dividing line around 400 nm. Additionally, the solid-state fluorescence spectroscopy results, depicted in Supplementary Figure 3, demonstrated a positive connection between the upregulated fluorescence emission intensity in the 1.6 g and 1.8 g ZnO-doped groups and the increased excitation wavelength. Conversely, the fluorescence emission spectra of the 2.0 g ZnO-doped group exhibited distinct bimodal emissions, which markedly differed from our previous study.[22] Given these findings, the 1.6 g ZnO-doped group was selected for the subsequent experiments.

As demonstrated in Figure 1C and D, the TEM images clearly illustrated the morphology of spherical CDs/ZnO and foamed CDs/ZnO. Compared to the result of our previous study,[22] the morphology of CDs/ZnO remained unchanged after the
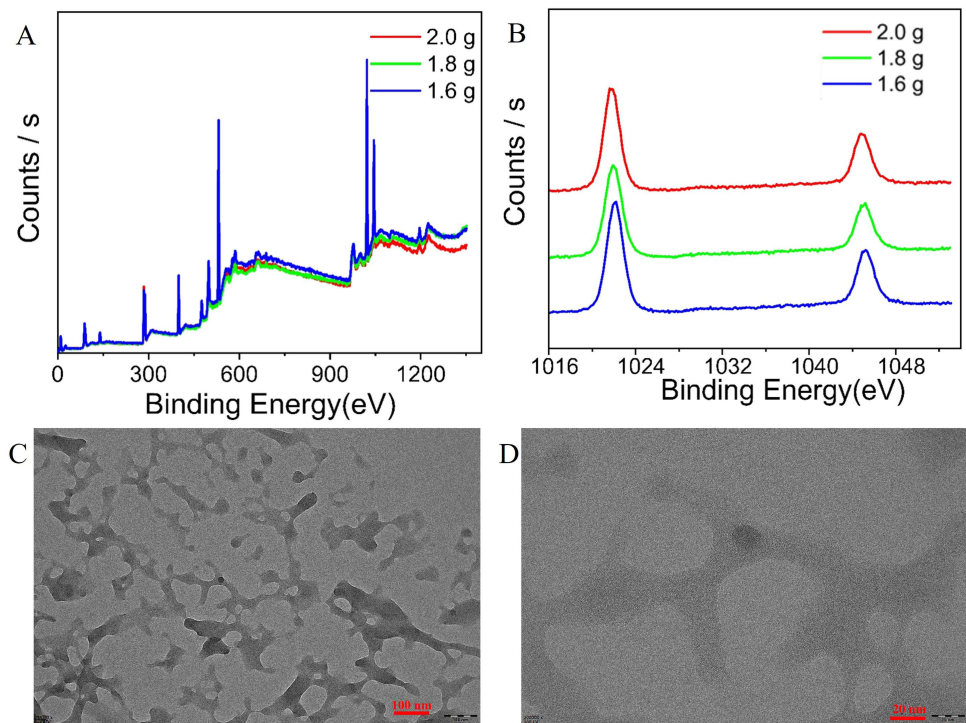
Figure 1 Characteristics of CDs/ZnO. (**A**) Full XPS surveys of CDs/ZnO from the 1.6 g, 1.8 g, and 2.0 g ZnO-doped groups, (**B**) Zn-2p region of CDs/ZnO from the 1.6 g, 1.8 g, and 2.0 g ZnO-doped groups. (**C**) TEM morphological of CDs/ZnO. (**D**) Enlarged TEM morphology of CDs/ZnO.

optimization of the synthesis pathway. Since the pore structure was not disrupted by the solvents, the distribution of CDs within the CDs/ZnO was sparser. Additionally, the fluorescence lifetime (τ) of the CDs/ZnO was analyzed using the fluorescence decay curve, and the results confirmed the average lifetime of CDs/ZnO was approximately 0.64 ns (Supplementary Figure 4).

Biocompatibility Assessment of CDs/ZnO

After the CDs/ZnO treatment, the biocompatibility of CDs/ZnO was corroborated by the in vitro culture models of GES-1, KGN, and MCF 10A cells. Compared with the NC group, the absence of impaired viabilities of GES-1 (Figure 2A–C), KGN (Figure 2D–F), and MCF 10A (Figure 2G–I) cells in the CDs/ZnO groups emphasizes the commendable biocompatibility of CDs/ZnO prepared in the present study.

As depicted in Figure 3, the evaluation of blood parameters confirmed the non-significant correlations between the CDs/ZnO treatments and the mouse renal/liver functions, evidenced by the non-discernible differences found in the levels of AST (Figure 3A, $P>0.05$), ALT (Figure 3B, $P>0.05$), BUN (Figure 3C, $P>0.05$), CRE (Figure 3D, $P>0.05$), TG (Figure 3E, $P>0.05$), and TC (Figure 3F, $P>0.05$) between the NC and CDs/ZnO groups. After the histological staining of H&E staining (Figure 3G), Masson trichrome staining (Figure 3H), and PAS staining (Figure 3I), no pathological damages were found to the liver, kidney, and spleen tissues of the CDs/ZnO group. These insights effectively reflect the exceptional biocompatibility of CDs/ZnO.

Table 1 Element Content in CDs/ZnO

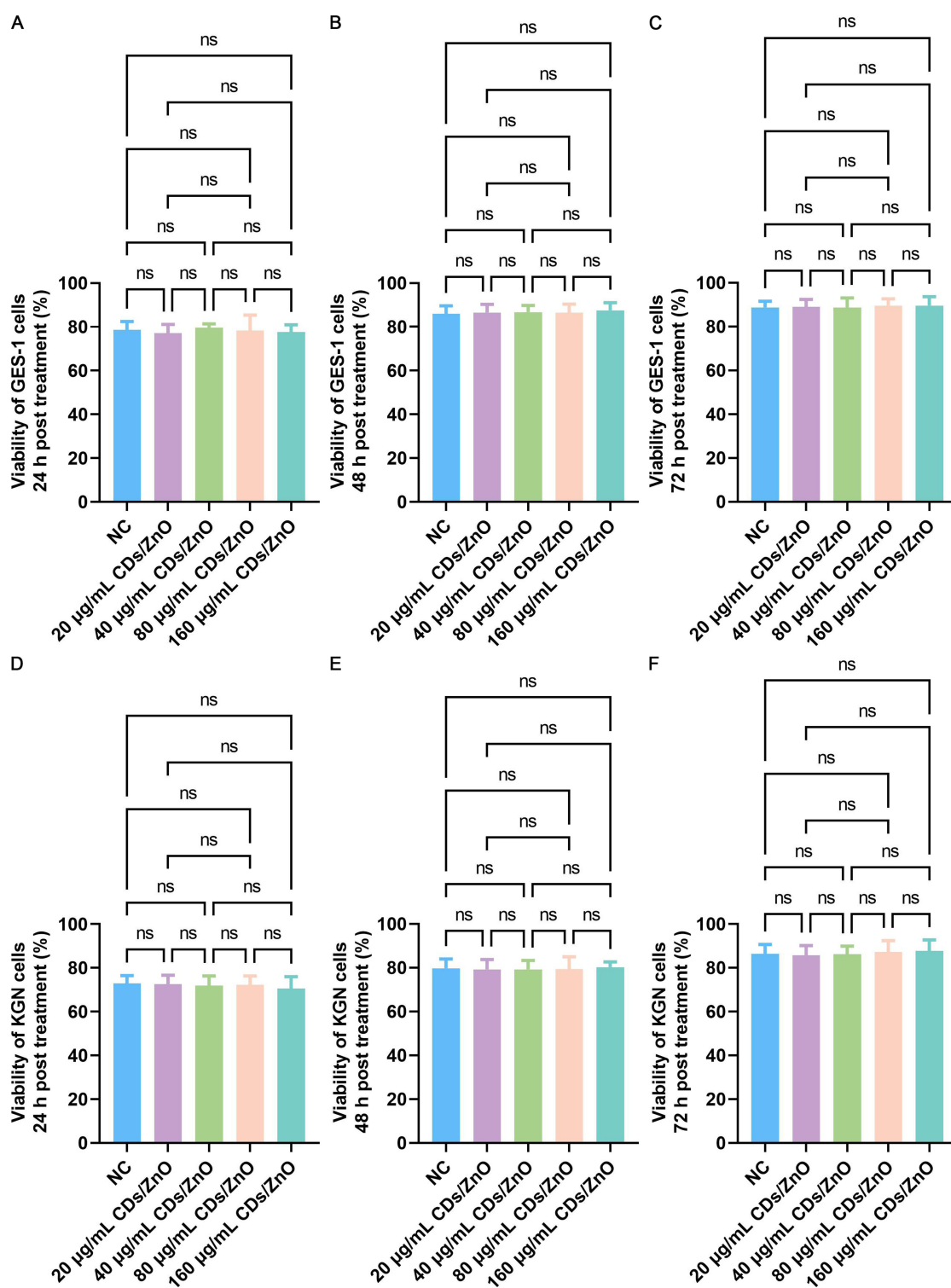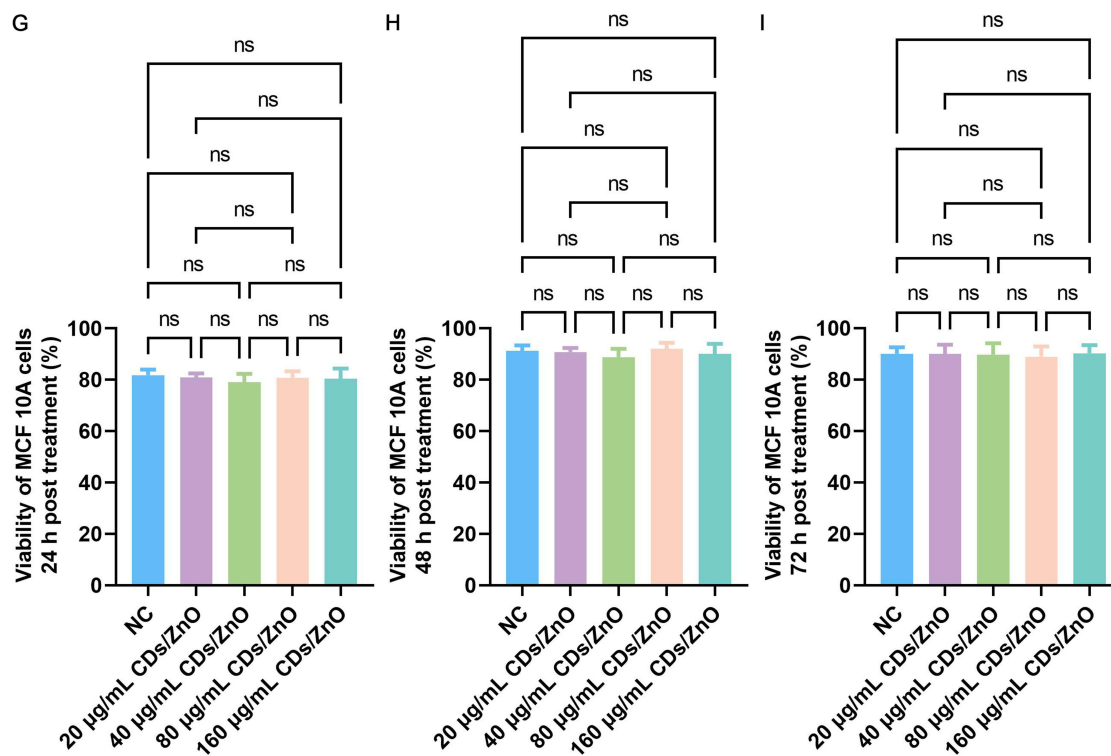| Element (%)	Carbon	Nitrogen	Oxygen	Zinc
1.6 g ZnO-doped group	26.32	29.26	39.25	5.16
1.8 g ZnO-doped group	29.9	27.79	37.18	5.13
2.0 g ZnO-doped group	33.8	32.29	30.20	3.71

Figure 2 Continued.

Figure 2 In vitro biocompatibility assessment of CDs/ZnO. (**A**) Viability of GES-1 cells treated with CDs/ZnO after 24 h. (**B**) Viability of GES-1 cells treated with CDs/ZnO after 48 h. (**C**) Viability of GES-1 cells treated with CDs/ZnO after 72 h. (**D**) Viability of KGN cells treated with CDs/ZnO after 24 h. (**E**) Viability of KGN cells treated with CDs/ZnO after 48 h. (**F**) Viability of KGN cells treated with CDs/ZnO after 72 h. (**G**) Viability of MCF 10A cells treated with CDs/ZnO after 24 h. (**H**) Viability of MCF 10A cells treated with CDs/ZnO after 48 h. (**I**) Viability of MCF 10A cells treated with CDs/ZnO after 72 h. ns represents $P>0.05$.

Effect of CDs/ZnO Treatments on Inhibiting the Malignant Behaviors of MDA-MB-231 Cells

The theranostics effects of CDs/ZnO treatments on the malignant TNBC progression were assessed by analyzing the viability, proliferation, migration, invasion, adhesion, clonogenicity, cell cycle distribution, apoptosis, and EMT progression of MDA-MB-231 cells.

MTT assay results indicated that the 24 h of incubation of CDs/ZnO gradually decreased the viabilities of MDA-MB-231 cells in a dose-dependent manner (Supplementary Figure 5, $P<0.05$) when compared to the NC group, implying the anti-tumor effect of CDs/ZnO treatments on MDA-MB-231 cells by its anti-proliferative mechanisms. Considering the statistical differences in the cell viability among the experimental groups, an optimal concentration of 80 μg/mL CDs/ZnO was selected as the optimal group for the following assessments.

Next, the results of the wound-healing assessment unveiled that the anti-migration effect of CDs/ZnO treatments significantly inhibited the scratch closure potentials of MDA-MB-231 compared with those of the NC group (Figure 4A and B, $P<0.05$). Simultaneously, the visual results of invasion and clonogenicity assessments promisingly indicated that the CDs/ZnO treatments not only decreased the number of migrated MDA-MB-231 cells (Figure 4C and D, $P<0.05$) but also restrained the number of immobilized MDA-MB-231 cells compared to the NC group (Figure 4E and F, $P<0.05$). Notably, greatly diminished number of adhesion (Figure 4G and H, $P<0.05$), altered cell cycle arrest (Figure 4I and J), and disturbed expression patterns of EMT-related proteins including E-cadherin, Vimentin, and SLUG (Figure 4M and N, $P<0.05$), were found in the CDs/ZnO treated MDA-MB-231 cells, in turns collectively supporting the idea that the CDs/ZnO exerts excellently anti-metastatic performances on MDA-MB-231 cells.

Importantly, in line with these above results related to the anti-metastatic effect of CDs/ZnO treatments, the proapoptotic effect of CDs/ZnO treatments on the MDA-MB-231 cells was subsequently confirmed by the consistent
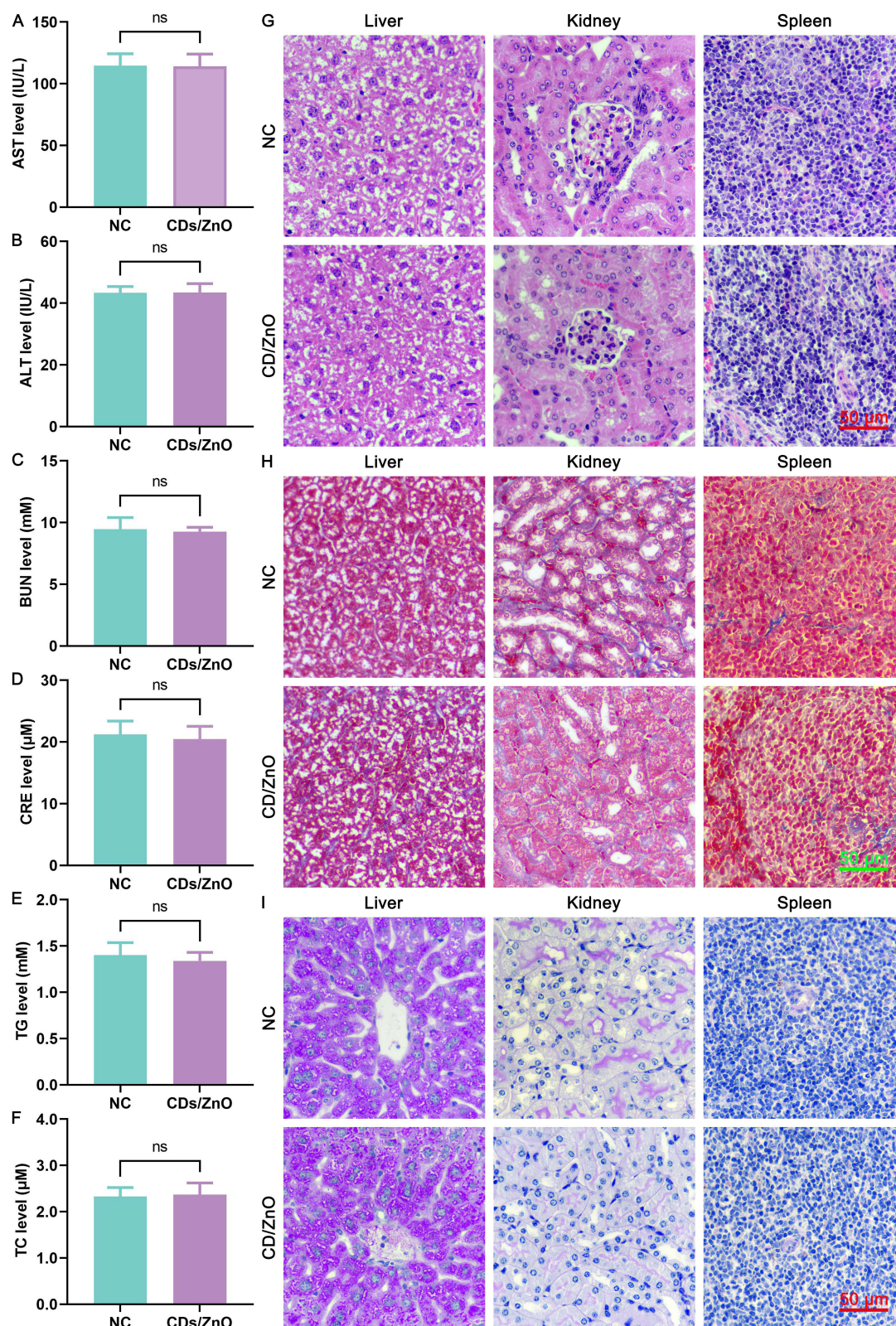
Figure 3 In vivo biocompatibility assessment of CDs/ZnO. (**A**) AST level. (**B**) ALT level. (**C**) BUN level. (**D**) CRE level. (**E**) TG level. (**F**) TC level. (**G**) H&E staining. (**H**) Masson trichrome staining. (**I**) PAS staining. ns represents P>0.05.
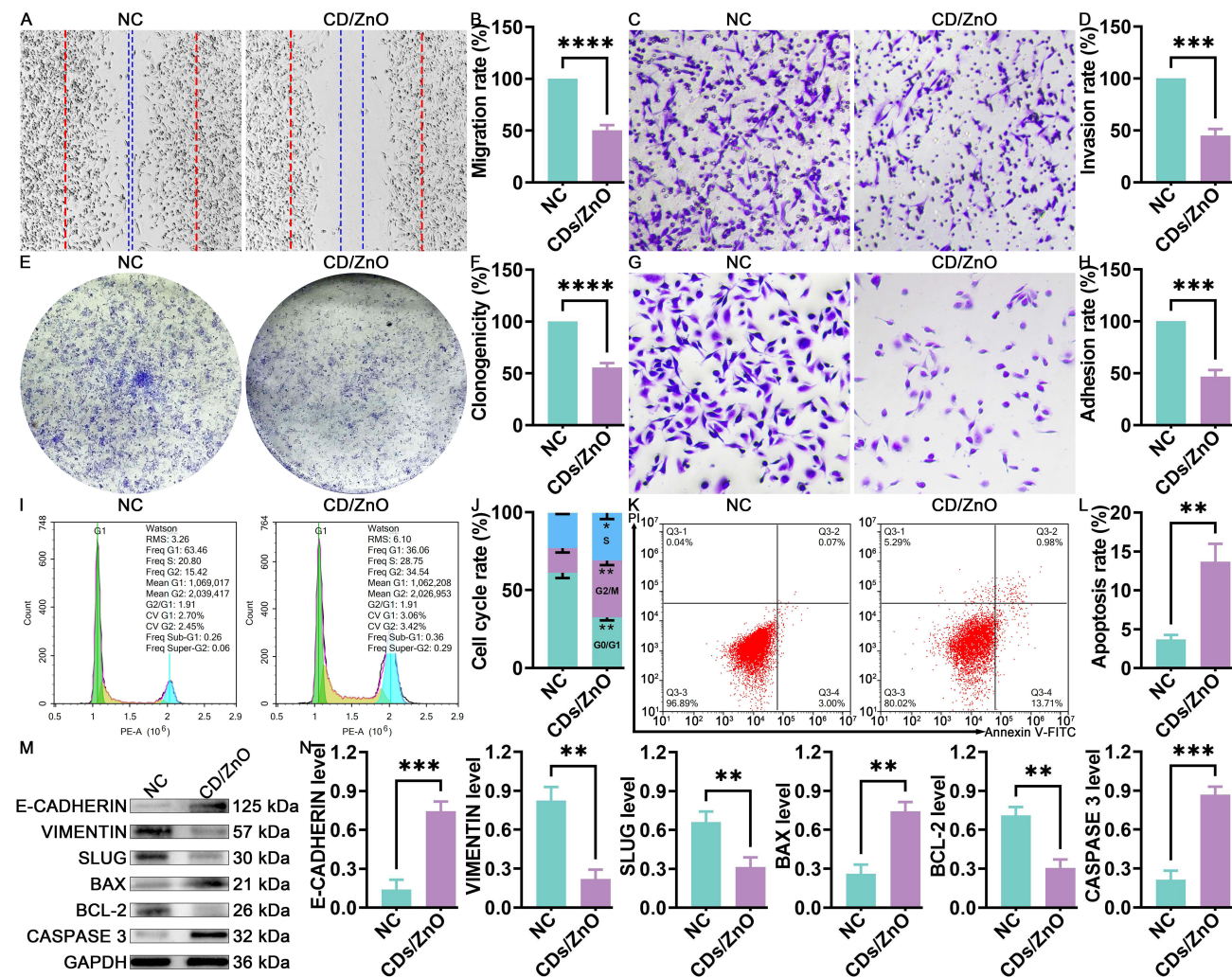
Figure 4 Effect of CDs/ZnO treatments on inhibiting the malignant behaviors of MDA-MB-231 cells. (**A**) Representative result of cell migration. (**B**) Quantitative result of cell migration. (**C**) Representative result of cell invasion. (**D**) Quantitative result of cell invasion assay. (**E**) Representative result of clonogenicity assay. (**F**) Quantitative result of clonogenicity assay. (**G**) Representative result of cell adhesion. (**H**) Quantitative result of cell adhesion assay. (**I**) Cell cycle distribution. (**J**) Percentage of cells in each cell cycle phase. (**K**) Representative FACS result of Annexin V/PI staining. (**L**) Apoptosis rate. (**M**) Representative expression result of EMT-related proteins. (**N**) Relative expression levels of ETM-related proteins. * represents P<0.05, with ** representing P<0.01, *** representing P<0.001, and **** representing P<0.0001.

differences in the Annexin V staining signals (Figure 4K and L, P<0.05) and expression patterns of BAX, BCL-2, and Caspase 3 (Figure 4M and N, P<0.05) between the NC and CDs/ZnO groups, initially emphasizing the depressed effect of CDs/ZnO treatments on perturbing the malignant TNBC progression by instigating the cellular apoptosis.

Effect of CDs/ZnO Treatments on Inducing the Redox Imbalance of MDA-MB-231 Cells

Compared with the NC group, microscopic observation of enhanced DCFH-DA staining intensity in the CDs/ZnO group emphasized the elevated ROS levels generated in the CDs/ZnO treated MDA-MB-231 cells (Figure 5A and B, P<0.05). Additionally, the presence of diminished MitoTracker staining intensity (Figure 5C and D, P<0.05) and altered ΔΨm potential (JC-1 ratio, Figure 5E and F, P<0.05) in the CDs/ZnO group effectively reflected the mitochondrial dysfunctions in the CDs/ZnO treated MDA-MB-231 cells.

Furthermore, the oxidative stress-related damages induced by the CDs/ZnO treatments were determined by assessing the biochemical content including SOD, GSH, CAT, MDA, LDH, and ATP in MDA-MB-231 cells. Our results indicated that the levels and activities of SOD (Figure 5G, P<0.05), GSH (Figure 5H, P<0.05), CAT (Figure 5I, P<0.05), and ATP

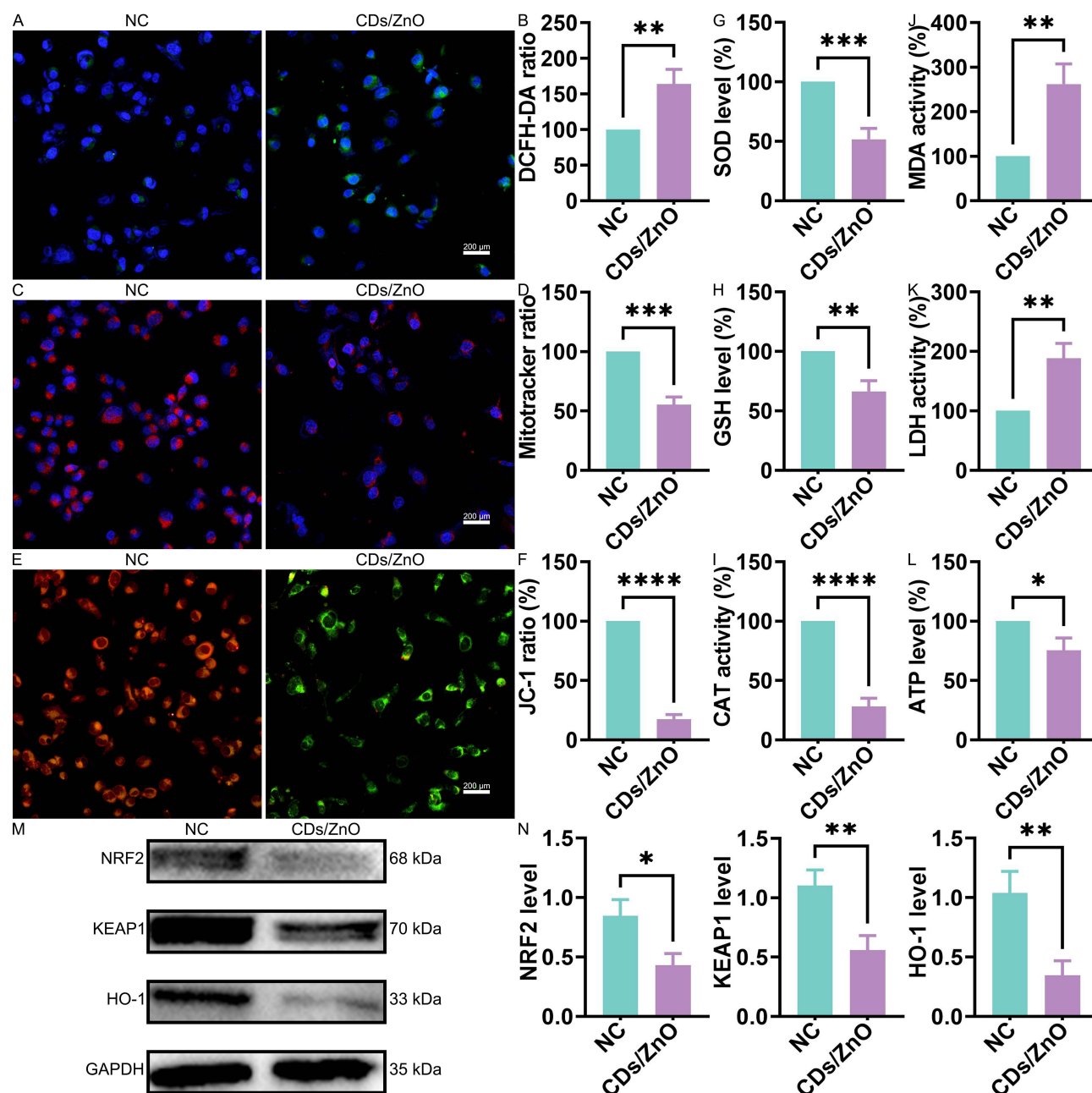**Figure 5** Effect of CDs/ZnO treatments on inducing the redox imbalance of MDA-MB-231 cells. (**A**) Representative result of DCFH-DA staining. (**B**) Quantitative result of DCFH-DA staining. (**C**) Representative result of MitoTracker staining. (**D**) Quantitative result of MitoTracker staining. (**E**) Representative result of JC-1 staining. (**F**) Quantitative result of JC-1 staining. (**G**) SOD level. (**H**) GSH level. (**I**) CAT activity. (**J**) MDA activity. (**K**) LDH activity. (**L**) ATP level. (**M**) Representative expression result of redox homeostasis-related proteins. (**N**) Relative expression levels of redox homeostasis-related proteins. * represents P<0.05, with ** representing P<0.01, *** representing P<0.001, and **** representing P<0.0001.

(Figure 5L, P<0.05) were significantly reduced upon exposure to CDs/ZnO treatments. It is worth mentioning that the MDA (Figure 5J, P<0.05) and LDH level (Figure 5K, P<0.05) in the CDs/ZnO group were remarkably promoted in comparison with that of the NC group. And the altered expression levels of redox homeostasis-related proteins between the NC and CDs/ZnO groups (Figure 5M and N, P<0.05) compellingly confirmed that the CDs/ZnO treatments effectively induced the oxidants generation, then collectively reaffirming the therapeutic effect of CDs/ZnO treatments against TNBC progression by disrupting the redox homeostasis of TNBC cells, thus shifting it towards cytotoxic oxidation.

Effect of CDs/ZnO Treatments on Inducing the Metabolome Disturbances of MDA-MB-231 Cells

On the basis of prototype results, a multivariate analysis comparing the different metabolites of MDA-MB-231 cells between the NC and CDs/ZnO groups was performed to elucidate the potential effects of CDs/ZnO treatment on inducing the metabolome disturbances of MDA-MB-231 cells.

As illustrated in Figure 6A–C, the score plots from the PCA and PLS-DA models clearly demonstrated notable differences between the NC and CDs/ZnO groups in both positive and negative ion modes, suggesting significant metabolic differences in the MDA-MB-231 cells between the NC and CDs/ZnO groups.

In addition, a total of 267 significantly different metabolites were identified in the positive ion modes (n = 176, Figure 6D and F) and negative ion modes (n = 149, Figure 6E and G) between the NC and CDs/ZnO groups. Subsequently, metabolic pathway enrichment analysis was performed for the differential metabolites in positive and negative ion modes. The results confirmed that the significantly different metabolites between the NC and CDs/ZnO groups were mainly enriched in the pathways such as MAPK signaling pathway, choline metabolism in cancer, necroptosis, FoxO signaling pathway, citrate cycle, glutamatergic synapse, metabolic pathways, glutathione metabolism, HIF-1 signaling pathway, and oxidative phosphorylation (Figure 6H).

Effect of CDs/ZnO Treatments on Triggering the Transcriptome Alterations of MDA-MB-231 Cells

To uncover the molecular features underlying the therapeutic effect of CDs/ZnO treatments against TNBC progression, the transcriptome characteristics of MDA-MB-231 cells upon CDs/ZnO exposure were analyzed. The results confirmed a total of 128,903 transcripts were mined in the MDA-MB-231 cells between the NC and CDs/ZnO groups. As visualized in Figure 7A, the volcano plot showed that 1210 DEGs were statistically identified in both NC and CDs/ZnO groups, comprising 382 upregulated DEGs and 828 downregulated DEGs in the CDs/ZnO group when compared to the NC group (P<0.05). As expected, the heat map, shown in Figure 7B, confirmed that the MDA-MB-231 cells treated with CDs/ZnO had a distinct hierarchical clustering of genes compared to the NC group.

Conventionally, the functional enrichment analyses of GO were performed to determine the overall functional implications of these identified DEGs in the CDs/ZnO-treated MDA-MB-231 cells. In terms of biological processes (BP, Figure 7C), these identified DEGs were predominantly involved in the subcategories of cell adhesion, cell migration, and negative regulation of growth, which was significantly consistent with the pronounced functional phenotypes in the MDA-MB-231 cells upon CDs/ZnO exposure. Additionally, these identified DEGs were significantly implicated in cellular component (CC) terms such as cytoskeleton, extracellular matrix, and focal adhesion (Figure 7C). Regarding molecular function (MF), these DEGs were associated with growth factor activity, metalloendopeptidase activity, and fibronectin binding (Figure 7C). Importantly, KEGG pathways associated with estrogen signaling pathway, small cell lung cancer, basal cell carcinoma, hippo signaling pathway, MAPK signaling pathway, NF κ B pathway, and cytokine-cytokine receptor interaction were significantly enriched in the CDs/ZnO-treated MDA-MB-231 cells (Figure 7D).

Additionally, quantitative assessments of the Western blot of MAPK signaling pathways-related proteins were performed to validate the data accuracy of the metabolome and transcriptome. As expected, the expression results of MAPK signaling pathways-related proteins in the CDs/ZnO-treated MDA-MB-231 cells, depicted in Supplementary Figure 6A and B, corresponded well with these former studies, in turn confirming the result reliability of the metabolome and transcriptome.

In vivo Anti-Cancer Effect of CDs/ZnO Treatments Against TNBC Progression

Encouraged by the above therapeutic effects of CDs/ZnO treatment against TNBC progression, the anti-tumor effect of CDs/ZnO treatment against TNBC progression was confirmed by the in vivo models. As expected, the CDs/ZnO treatment significantly inhibited the in vivo tumor growth (Figure 8A), as evidenced by the notable differences in the tumor volume (Figure 8B, P<0.05) and weight (Figure 8C, P<0.05) between the NC and CDs/ZnO groups.

To illustrate that CDs/ZnO attenuates TNBC progression, the expression levels of KI-67 and VEGF were also examined, as well as the cell apoptosis assessment by Tunel staining. The results showed that the expression levels of KI-
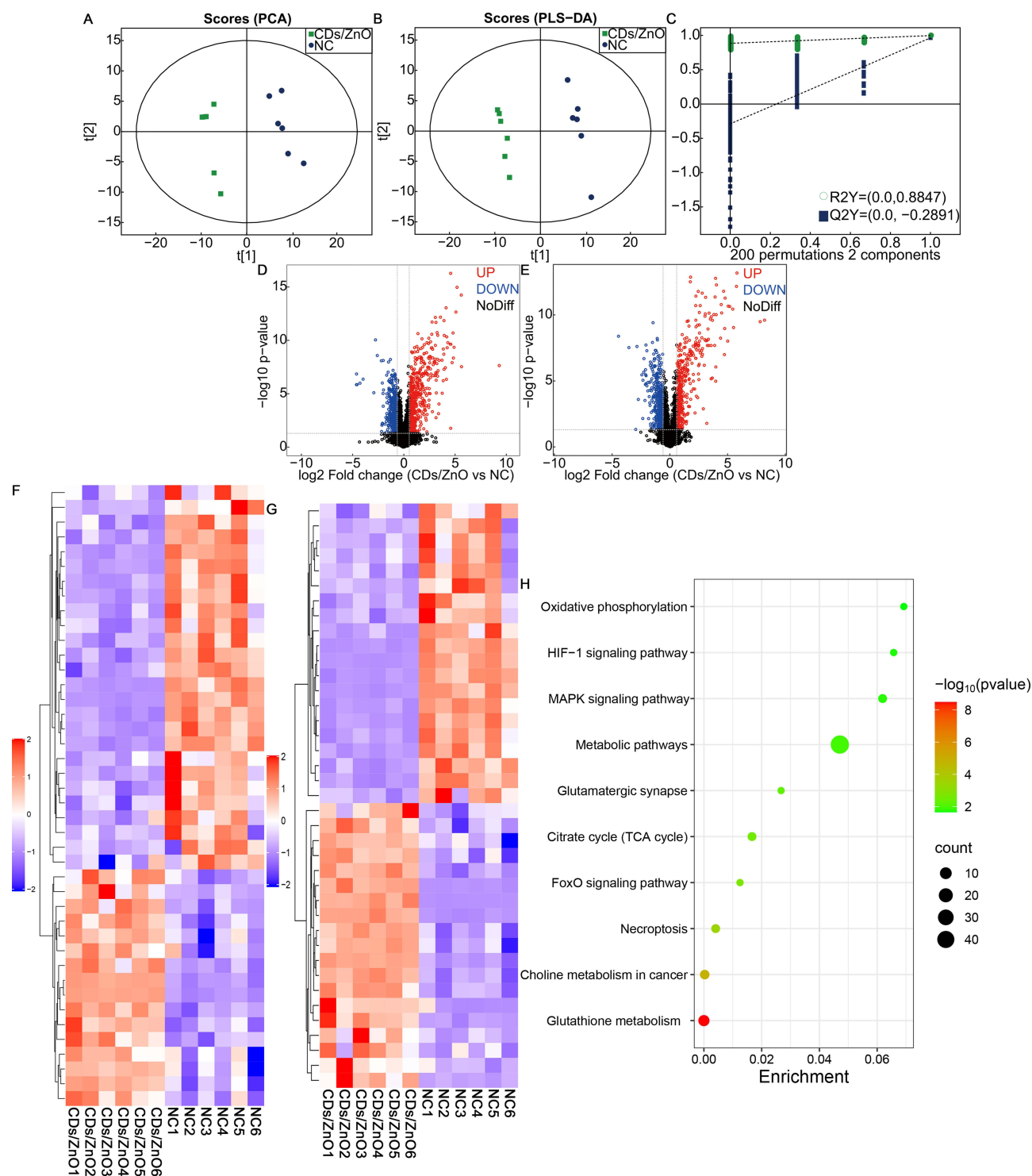
Figure 6 Effect of CDs/ZnO treatments on inducing the metabolome disturbances of MDA-MB-231 cells. (**A**) PCA score plot. (**B**) Score plot of PLS-DA. (**C**) Permutation plot of PLS-DA. (**D**) Volcano plots of differential metabolites in positive ion mode. (**E**) Volcano plots of differential metabolites in negative ion mode. (**F**) Heat map of differential metabolites in positive ion mode. (**G**) Heat map of differential metabolites in negative ion mode. (**H**) KEGG pathway enrichment analysis.

67 (Figure 8D and E, P<0.05) and VEGF (Figure 8F and G, P<0.05) were significantly reduced after CDs/ZnO treatment. Combined with the differences in the Tunel staining ratio between the NC and CDs/ZnO groups (Figure 8H and I, P<0.05), these results suggested that the CDs/ZnO treatment effectively inhibited the malignant TNBC progression.

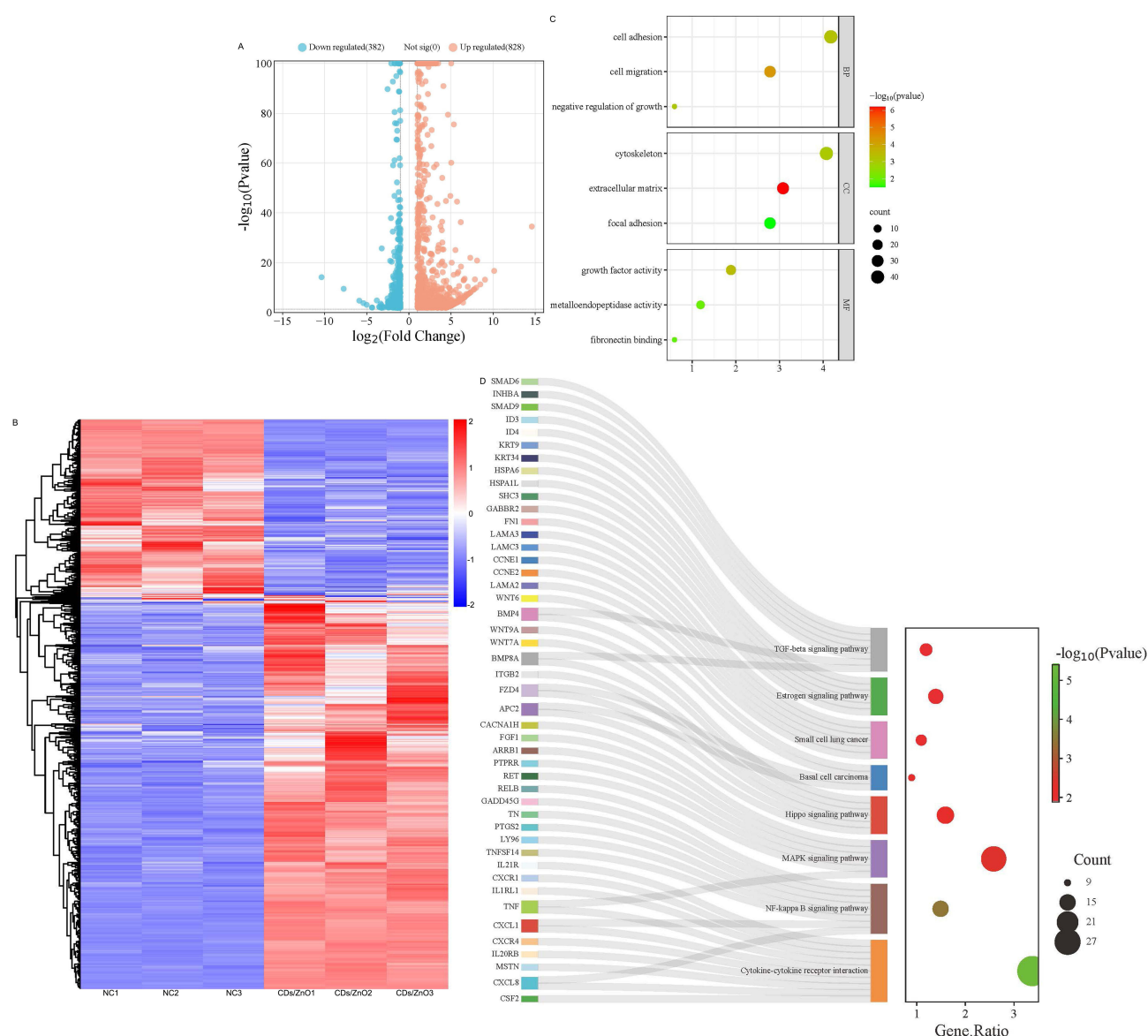**Figure 7** Effect of CDs/ZnO treatments on triggering the transcriptome alterations of MDA-MB-231 cells. (**A**) Volcano plots of DEGs. (**B**) Heat map of DEGs. (**C**) GO analysis. (**D**) KEGG pathway enrichment analysis.

Discussion

As an essential trace element to meet the cellular demands of bioenergetic, synthetic, and catabolic equilibrium, zinc is primarily acquired from the diet, absorbed in the intestine, and distributed to various target organs throughout the body.[30] As a key constituent or cofactor of more than 300 mammalian proteins, zinc plays crucial roles in numerous physiological processes, including enzyme function, gene expression, antioxidant defense, glycolipid metabolism, DNA metabolism, signal transduction, immune functions, cellular proliferation, meiotic maturation, apoptosis, and many other physiological procedures.[31,32] Additionally, a plethora of extensive studies have substantiated that, in response to extracellular stimuli, zinc functions not only as an intracellular signaling molecule to facilitate the transduction of signaling cascades but also as an intracellular secondary messenger for cell-to-cell communications, in turn influencing the proliferation, differentiation, and apoptosis of mammalian cells.[32]

Regardless of the delicately precise regulation mechanism involving a network of proteins, the imbalanced metabolism of intracellular zinc, including altered absorption, trafficking, utilization, storage, and expulsion, has been linked to various pathologies, such as immunodeficiency, cachexia, atrophy, diabetes, diarrhea, colitis, and neurodegenerative
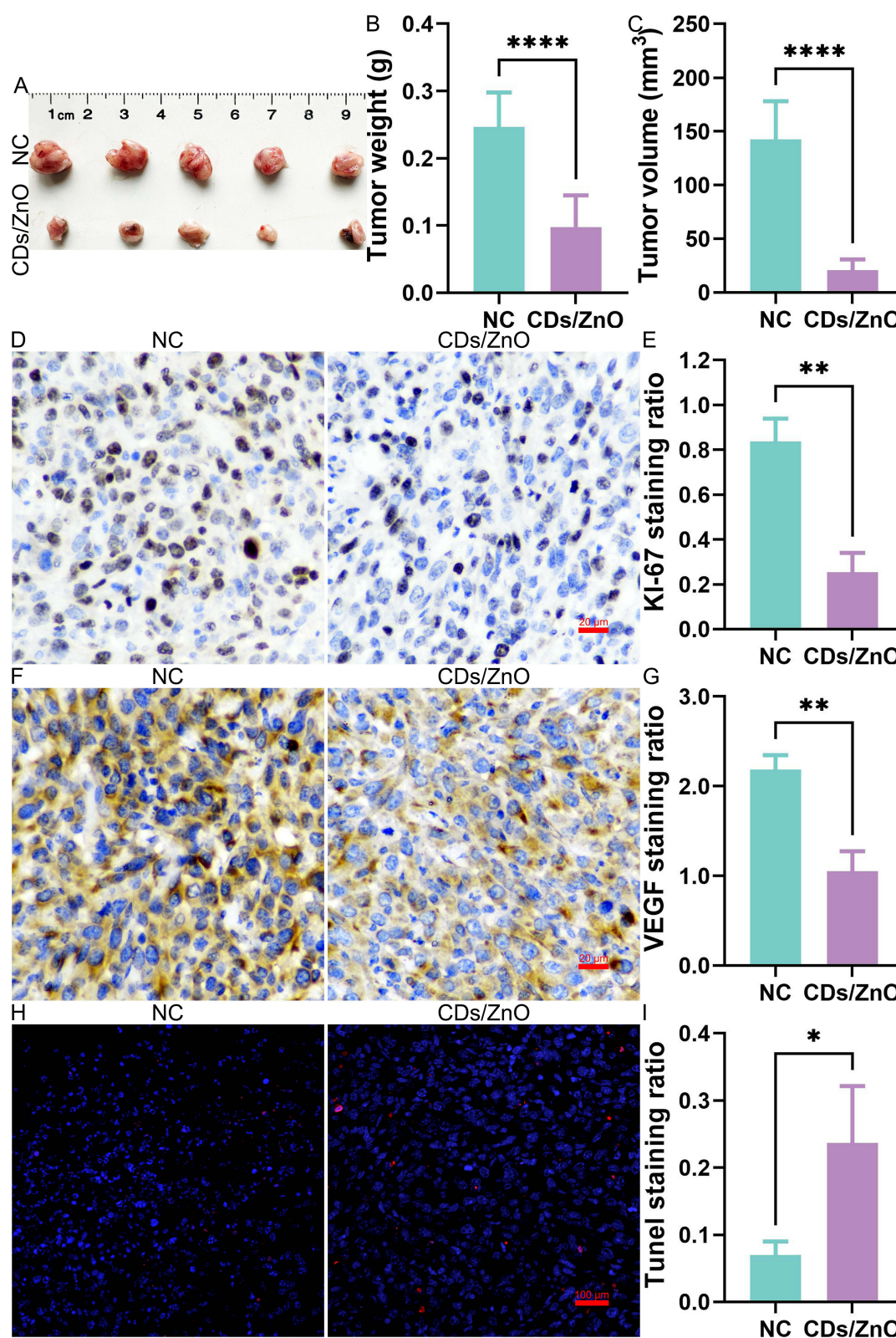
Figure 8 In vivo anti-cancer effect of CDs/ZnO treatments against TNBC progression. (**A**) Representative morphology of xenograft tissues. (**B**) Quantitative result of tumor volume. (**C**) Quantitative result of tumor weight. (**D**) Representative IHC staining result of KI-67. (**E**) Quantitative IHC staining result of KI-67. (**F**) Representative IHC staining result of VEGF. (**G**) Quantitative IHC staining result of VEGF. (**H**) Representative result of Tunel staining. (**I**) Quantitative result of Tunel staining. * represents P<0.05, with ** representing P<0.01, and **** representing P<0.0001.

diseases.[32,33] Numerous studies over the past decades have highlighted the positive relationships between altered serum zinc levels and the progression of diseases, such as epilepsy, obesity, multiple sclerosis, heart failure, gestational diabetes, and carcinogenesis.[34] According to these pharmaceutical studies revealing zinc deficiency as a risk factor for cancer development, the dietary restoration of zinc has been proposed as an alternative approach for cancer treatment.[35] It is of interest that the administration of zinc compounds, such as zinc chloride, zinc gluconate, zinc acetate, or zinc sulfate, effectively inhibited the malignant progression of osteosarcoma, breast, prostate, liver, gastric, and colon cancers by inhibiting angiogenesis, cell proliferation, and cell invasion or by inducing chemosensitivity, apoptosis, and cell cycle arrest.[30,36] Concurrently, the zinc-L-carnosine, zinc-curcumin, or zinc-dictyophora indusiata polysaccharide complexes, showed effective anti-proliferative activities across a group of human cancer cell lines.[30,37]

In addition, the recent developments of zinc-related nanotechnology have garnered scientific attention and benefited the pharmaceutical applications of zinc-based nanoparticles.[30] During the past decades, evidence has accumulated that ZnO nanoparticles (ZnO-NPs), with high desulfurization accuracy, high tumor specificity, outstanding desulfurization ability, well biocompatibility, and less toxicity, show promising apoptosis-inducing effects in numerous cancers.[25] Besides the possibility of using ZnO-NPs alone as innovative anti-tumor agents, the drug delivery system based on polyethylene glycol and ZnO-NPs triggered the apoptosis of breast cancer cells.[38,39] Additionally, the combined NPs based on thymoquinone and ZnO-NPs inhibited the proliferation of cancer cells,[40] highlighting the potential clinical application potentials of ZnO-NPs. However, the possible effect of CDs/ZnO against TNBC progression remains more detailed studies. As hypothesized, the combined results in the current study effectively confirmed that the in vitro CDs/ZnO treatments promisingly decreased the viability, proliferation, migration, invasion, adhesion, and clonogenicity of MDA-MB-231 cells, but also induced the cell cycle arrest, redox imbalance, apoptosis, disturbed metabolome, and transcriptomic alterations of MDA-MB-231 cells. Moreover, the in vivo experiments confirmed the excellent anti-cancer effect of CDs/ZnO treatments.

As metal-free, quasi-spherical, and zero-dimensional nanoparticles with dimensions less than 10 nm, CDs have been considered the superior carbon members of the carbon nanomaterial family in recent years.[41] Due to their biological compatibility, excellent electrical conductivity, low toxicity, high productivity, light stability, dispersibility, sustainability, and economic benefits for synthesis, CDs have shown great potential in biomedical applications such as anti-cancer, antioxidant, biosensing, drug delivery, bioimaging, anti-microbial, photoluminescence, osteogenesis, and bioimaging, etc.[42,43] Besides these above advantages, the properties and processability of CDs were effectively regulated when functionalized with special ligands such as ions, polymers, organic molecules, proteins, and DNA by chemical doping and surface modification strategies.[41,44] Intriguingly, extensive studies have confirmed that non-metal doping with dopants like boron, chloride, fluorine, iodine, nitrogen, phosphorus, selenium, silicon, sulfur, and tellurium, and metal doping with copper, cobalt, europium, gadolinium, hafnium, iron, lanthanide, manganese, nickel, silver, and zinc, effectively regulate the intrinsic structure and surface state of CDs, and simultaneously, change the physical and optical properties of multifunctional CDs.[44,45] These previous publications have confirmed that the effective introductions of CDs in ZnO not only benefit the photoelectrocatalytic efficacy of CDs/ZnO but also offer excellent promises for the sensitive detection of cancer cells and cancer cell-based drug delivery systems.[46–48] In contrast, the biosafety challenges remain with other nanomaterials, such as the leakage of calcium from calcium carbonate nanomaterials in body fluids, cardiac toxicity induced by iron oxide NPs, and the inflammatory effects of selenium nanoparticles, which complicate the accurate assessment of their biosafety.[49,50] Additionally, copper-based nanomaterials face limitations, including high cost, inadequate mechanical strength, and difficulties with substrate coating, which hinder their broader application from the laboratory to clinical use and commercialization in medical facilities today.[51,52] In comparison, ZnO exhibits excellent biocompatibility and a high toxicity threshold, reducing the risks for genetic disorders, liver dysfunction, renal failure, and neurological deficits typically associated with the excessive accumulation and toxicity of other trace elements, such as calcium, copper, iron, selenium, etc.[53–55]

In 2024, Dong et al designed the nano heterostructures of gold nanorods inherent to ZnO with CDs doping (Au@ZnO@CDs), and they found that the functionalized modification of Au@ZnO@CDs by hyaluronic acid exhibited excellent photothermal therapy (PDT) efficacy of TNBC progression.[56] However, the potential effect of CDs/ZnO alone on the treatment of TNBC progression requires more detailed investigations to confirm and expand the clinical

application potentials of CDs/ZnO. In the present study, CDs/ZnO were synthesized with citric acid applied as the carbon source, urea applied as the nitrogen source, and ZnO used as a reactive dopant. We found that the CDs/ZnO treatments effectively decreased the viability, proliferation, migration, invasion, adhesion, and clonogenicity of MDA-MB-231 cells but also induced the cell cycle arrest, apoptosis, disturbed metabolome, and transcriptomic alterations of MDA-MB-231 cells. Combined with the enhanced apoptosis, decreased proliferation, and suppressed angiogenesis potentials of 4T1 cells, these results promisingly confirm the excellent anti-cancer potency of CDs/ZnO against TNBC progression by disrupting the malignant behaviors of breast cancer cells.

In addition, we found significant redox imbalances in the CDs/ZnO-treated MDA-MB-231 cells, as evidenced by the significant differences in the ROS production, mitochondrial functions, antioxidant enzyme activities, and protein expressions of NRF2, KEAP1, and HO-1 between the NC and CDs/ZnO groups. As described as the chemical species formed upon the incomplete reduction of oxygen, ROS mainly includes superoxide anion, singlet oxygen, hydrogen peroxide, and hydroxyl radical.[57] ROS acts as a second messenger in the regulation of various physiological functions in mammalian cells, comparatively, the ROS disequilibrium beyond the cellular tolerability thresholds leads to oxidative stress, which is implicated in the incidences of consequent diseases such as aging, carcinogenesis, atherosclerosis, infection, inflammation, reproductive failure, and neurodegenerative disease.[58–60] Consistent with our former publication,[24] mounting evidences has also confirmed the therapeutic target applications of overproduction of ROS against TNBC progression via multiple signal transduction pathways such as initiating the breakage of the DNA double-strand, triggering mitochondrial DNA mutation, inducing impairment of mitochondrial electron transport system (ETS), enhancing lipid peroxidation, decreasing ATP production, boosting iron ferritinophagy, and promoting cell apoptosis.[61,62] Considering the key role of ROS in carcinogenesis, these ROS-related therapeutic modalities, such as chemodynamic therapy, controlled drug release therapy, photodynamic therapy, sono-dynamic therapy, and radiotherapy, have been preliminarily developed.[57,63] Along with the development of these aforementioned therapeutic paradigms, numerous ROS-based cancer nanoplatforms have also been fabricated.[57] Partly consistent with these former publications revealing the anti-cancer effect of ZnO-based NPs treatments on promoting the ROS production level in the acute myeloid leukemia cells,[64] epithelial carcinoma cells,[65,66] lung cancer cells,[67–69] colon cancer cells,[70,71] prostate cancer cells,[70] diffuse large B-cell lymphoma cells,[72] epidermoid cancer cells,[73] breast cancer cells,[74] gastric cancer cells,[75,76] bone cancer cells,[77] melanoma cells,[78,79] hepatocellular cancer cells,[80] and laryngeal cancer cells,[81] elevated ROS production levels in the CDs/ZnO-treated MDA-MB-231 cells were found in the present study, in turns suggesting the promising therapeutic application of CDs/ZnO against TNBC progression via promoting ROS productions.

Lastly, the disturbed metabolome and transcriptome alterations in the CDs/ZnO-treated MDA-MB-231 cells confirmed the anti-cancer effect of CDs/ZnO treatments against TNBC progression was positively related to the regulation of the MAPK signaling pathway. As highly conserved tertiary kinase cascades, the MAPK signaling pathway consists of three sequentially acting kinases, the upstream kinase MAPK kinase kinase (MAPKKK), the intermediate kinase MAPK kinase (MAPKK), and the downstream kinase MAPK.[82] The multiple intracellular and extracellular stressors, such as growth factors, inflammatory cues, cytokine stimulation, genotoxic damage, environmental factors, and oxidative stress, stimulate MAPKKK, which in turn activate corresponding MAPKK and MAPK, and further regulate biological processes including oncogenic transformation, proliferation, differentiation, apoptosis, angiogenesis, senescence, metastasis, and metabolism.[82,83] Consequently, various protein kinases in the MAPK signaling pathway have been confirmed as predictive biomarkers for multiple cancers.[82] In addition, these MAPK pathway-related therapeutics, such as binimetinib, cobimetinib, donafenib tosylate, pirfenidone, selumetinib sulfate, trametinib, and tivozanib have already been approved for clinical cancer treatment.[82]

Additionally, these former studies have solidly confirmed the positive connections between zinc homeostasis and the regulation of MAPK signaling pathway.[84,85] For example, Zhang et al found that the intracellular liberation and accumulation of zinc contributed to the ATP depletion, mitochondrial membrane depolarization, and the activation of the MAPK signaling pathway, resulting in caspase-dependent apoptosis.[86] The increases in the intracellular zinc levels induce the activation of the MAPK signaling pathway, which was responsible for the demise of rat bone marrow mesenchymal stem cells (rBMSCs),[87] neuronal cells,[88] Hep-2 cells,[89] and mouse Sertoli cells.[90] Although the detailed regulation effect of CDs/ZnO treatments on the activation of the MAPK signaling pathway needs more exploration, we

hope the present study warrants more studies to analyze the regulation mechanism related to the anti-cancer potency of CDs/ZnO treatments against the malignant TNBC progression.

Conclusion

In this study, CDs/ZnO were successfully synthesized using citric acid as the carbon source, urea as the nitrogen source, and ZnO as a reactive dopant through microwave heating. The results demonstrate that CDs/ZnO exhibits favorable biosafety profiles and potent anti-cancer efficacy, particularly in inhibiting TNBC progression. By disrupting malignant behaviors of TNBC cells through modulation of the MAPK signaling pathway, the synthesized CDs/ZnO in the present study show promising potential for broader medical applications in cancer treatment.

Abbreviations

CDs/ZnO, zinc oxide-doped carbon dots; TNBC, triple-negative breast cancer; ZnO, zinc oxide; WHO, World Health Organization; ER, estrogen receptor; PR, progesterone receptor; HER2, human epidermal growth factor receptor 2; CQDs, carbon-based quantum dots; CDs, carbon dots; PDs, polymer dots; GQDs, graphene quantum dots; TEM, Transmission electron microscopy; XRD, X-ray diffraction; XPS, X-ray Photoelectron Spectroscopy; PL, photoluminescence; TRPL, time-resolved photoluminescence; NTAS, nanosecond transient absorption emission spectrometer; NC, negative control; ALT, alanine aminotransferase; AST, aspartate aminotransferase; BUN, blood urea nitrogen; CRE, creatinine; TG, triglyceride; TC, total cholesterol; H&E, Hematoxylin and eosin; PAS, Periodic acid Schiff; FBS, fetal bovine serum; P/S, penicillin and streptomycin antibiotics; MTT, 3-(4,5-dimethylthiazol-2-yl)-2,5-diphenyl tetrazolium bromide; DPBS, Dulbecco's phosphate-buffered saline; DMSO, dimethyl sulfoxide solution; IR, inhibiting rate; FACS, flow cytometry; PI, propidium iodide; DCFH-DA, dichlorofluorescein diacetate; KEGG, Kyoto Genes and Genomes; DEGs, differentially expressed genes; FDR, false discovery rate; FC, fold change; GO, gene ontology; SDS-PAGE, sodium dodecyl sulfate-polyacrylamide gel; PVDF, polyvinylidene fluoride membranes; TBST, Tris-HCl solution supplemented with 0.1% Tween-20; ECL, enhanced chemiluminescence solution; IHC, immunohistochemistry; Tunel, Terminal Deoxynucleotidyl Transferase dUTP Nick End Labelling; BSA, bovine albumin solution; DAB, 3.3′-diaminobenzidine tetrahydrochloride; TdT, Terminal Deoxynucleotidyl Transferase; SD, standard deviation; SPSS, Statistical Package for the Social Sciences software; BP, biological processes; CC, cellular component; MF, molecular function; ZnO-NPs, ZnO nanoparticles; Au@ZnO@CDs, gold nanorods inherent to ZnO with CDs doping; PDT, photothermal therapy; ETS, electron transport system; MAPKKK, MAPK kinase kinase; MAPKK, MAPK kinase; rBMSCs, rat bone marrow mesenchymal stem cells.

Acknowledgments

Funding

Disclosure

All authors declare that they have no known competing financial interests or personal relationships that could have appeared to influence the work reported in this study.

References

1. Harris MA, Savas P, Virassamy B, et al. Towards targeting the breast cancer immune microenvironment. *Nat Rev Cancer*. 2024;24(8):554–577. doi:10.1038/s41568-024-00714-6

2. Delaloge S, Khan SA, Wesseling J, Whelan T. Ductal carcinoma in situ of the breast: finding the balance between overtreatment and under-treatment. *Lancet*. 2024;403(10445):2734–2746. doi:10.1016/S0140-6736(24)00425-2

3. Loibl S, Poortmans P, Morrow M, Denkert C, Curigliano G. Breast cancer. *Lancet*. 2021;397(10286):1750–1769. doi:10.1016/S0140-6736(20)32381-3

4. Britt KL, Cuzick J, Phillips K-A. Key steps for effective breast cancer prevention. *Nat Rev Cancer*. 2020;20(8):417–436. doi:10.1038/s41568-020-0266-x

5. Yuan P, Ma N, Xu B. Poly (adenosine diphosphate-ribose) polymerase inhibitors in the treatment of triple-negative breast cancer with homologous repair deficiency. *Med Res Rev*. 2024;44:2774–2792. doi:10.1002/med.22058

6. Cifuentes C, Oeste CL, Fernández-Pisonero I, et al. Unmutated RRAS2 emerges as a key oncogene in post-partum-associated triple negative breast cancer. *Mol Cancer*. 2024;23(1):142. doi:10.1186/s12943-024-02054-3

7. Derakhshan F, Reis-Filho JS. Pathogenesis of triple-negative breast cancer. *Ann Rev Pathol*. 2022;17(1):181–204. doi:10.1146/annurev-pathol-042420-093238

8. Cortes J, Rugo HS, Cescon DW, et al. Pembrolizumab plus chemotherapy in advanced triple-negative breast cancer. *N Engl J Med*. 2022;387(3):217–226. doi:10.1056/NEJMoa2202809

9. Rayson VC, Harris MA, Savas P, et al. The anti-cancer immune response in breast cancer: current and emerging biomarkers and treatments. *Trends Cancer*. 2024;10(6):490–506. doi:10.1016/j.trecan.2024.02.008

10. Li Y, Zhang H, Merkher Y, et al. Recent advances in therapeutic strategies for triple-negative breast cancer. *J Hematol Oncol*. 2022;15(1):121. doi:10.1186/s13045-022-01341-0

11. Huang H, Zheng Y, Chang M, et al. Ultrasound-based micro-/nanosystems for biomedical applications. *Chem Rev* 2024;124(13):8307–8472. doi:10.1021/acs.chemrev.4c00009

12. Wang H, Yang S, Chen L, et al. Tumor diagnosis using carbon-based quantum dots: detection based on the hallmarks of cancer. *Bioact Mater* 2024;33:174–222. doi:10.1016/j.bioactmat.2023.10.004

13. Zhang J, Ali K, Wang J. Research advances of lipid nanoparticles in the treatment of colorectal cancer. *Int J Nanomed*. 2024;19:6693–6715. doi:10.2147/IJN.S466490

14. Krasley AT, Li E, Galeana JM, Bulumulla C, Beyene AG, Demirer GS. Carbon nanomaterial fluorescent probes and their biological applications. *Chem Rev* 2024;124(6):3085–3185. doi:10.1021/acs.chemrev.3c00581

15. Du H, He L. Synergistic improvement of antioxidant and antibacterial properties of carbon quantum complexes with zinc doping and chlorogenic acid for longan preservation. *Food Chem*. 2024;439:138169. doi:10.1016/j.foodchem.2023.138169

16. Shen C-L, Liu H-R, Lou Q, et al. Recent progress of carbon dots in targeted bioimaging and cancer therapy. *Theranostics*. 2022;12(6):2860–2893. doi:10.7150/thno.70721

17. Sun L, Liu H, Ye Y, et al. Smart nanoparticles for cancer therapy. *Signal Transduction Targeted Ther*. 2023;8(1):418. doi:10.1038/s41392-023-01642-x

18. Miao Q, Qi J, Li Y, et al. Anchoring zinc-doped carbon dots on a paper-based chip for highly sensitive fluorescence detection of copper ions. *Analyst*. 2021;146(20):6297–6305. doi:10.1039/D1AN01268A

19. Mohapatro U, Mishra L, Mishra M, Mohapatra S. Zn-CD@Eu ratiometric fluorescent probe for the detection of dipicolinic acid, uric acid, and ex vivo uric acid imaging. *Anal Chem* 2024;96(21):8630–8640. doi:10.1021/acs.analchem.4c00708

20. Kumar VB, Lahav M, Gazit E. Preventing biofilm formation and eradicating pathogenic bacteria by Zn doped histidine derived carbon quantum dots. *J Mat Chem B*. 2024;12(11):2855–2868. doi:10.1039/D3TB02488A

21. Riahi Z, Khan A, Rhim J-W, Shin GH, Kim JT. Sustainable packaging film based on cellulose nanofibres/pullulan impregnated with zinc-doped carbon dots derived from avocado peel to extend the shelf life of chicken and tofu. *Int J Biol Macromol*. 2024;258:129302. doi:10.1016/j.ijbiomac.2024.129302

22. Wang M, Zhang K, Ji F, et al. CDs/ZnO composite material with solid state fluorescence performance for quantitative determination of methyl red content and antibacterial properties. *J Ind Eng Chem*. 2021;104:179–185. doi:10.1016/j.jiec.2021.08.021

23. Zhong Z, Zhang Y, Fu X, et al. Construction of photo-induced zinc-doped carbon dots based on drug-resistant bactericides and their application for local treatment. *Nanoscale Adv*. 2022;4(24):5365–5377. doi:10.1039/D2NA00375A

24. Wang M, Lan S, Zhang W, et al. Anti-cancer potency of copper-doped carbon quantum dots against breast cancer progression. *Int J Nanomed*. 2024;19:1985–2004. doi:10.2147/IJN.S449887

25. Pan X, Qi Y, Du Z, et al. Zinc oxide nanosphere for hydrogen sulfide scavenging and ferroptosis of colorectal cancer. *J Nanobiotechnol*. 2021;19(1):392. doi:10.1186/s12951-021-01069-y

26. Zhang W, Sun J, Liu F, et al. Alleviative effect of lactoferrin interventions against the hepatotoxicity induced by titanium dioxide nanoparticles. *Biol Trace Elem Res* 2023;202(2):624–642. doi:10.1007/s12011-023-03702-3

27. Zhang WQ, Sun JX, Lan ST, et al. Regulation of Fuzheng Huayu capsule on inhibiting the fibrosis-associated hepatocellular carcinogenesis. *J Asian Nat Prod Res*. 2024;26(10):1219–1238. doi:10.1080/10286020.2024.2355132

28. Li S, Yin Y, Dong X, et al. Protective effects of lactoferrin treatment against sodium arsenite exposure-induced nephrotoxicity. *Biol Trace Elem Res* 2024. doi:10.1007/s12011-024-04256-8

29. Jin Q, Liu G, Li S, et al. Decellularized breast matrix as bioactive microenvironment for in vitro three-dimensional cancer culture. *J Cell Physiol*. 2019;234(4):3425–3435. doi:10.1002/jcp.26782

30. Himoto T, Masaki T. Current trends on the involvement of zinc, copper, and selenium in the process of hepatocarcinogenesis. *Nutrients*. 2024;16(4):472. doi:10.3390/nu16040472

31. Schoofs H, Schmit J, Rink L. Zinc toxicity: understanding the limits. *Molecules*. 2024;29(13):3130. doi:10.3390/molecules29133130

32. Chen B, Yu P, Chan WN, et al. Cellular zinc metabolism and zinc signaling: from biological functions to diseases and therapeutic targets. *Signal Transduction Targeted Ther*. 2024;9(1):6. doi:10.1038/s41392-023-01679-y

33. Prasad AS. Discovery of human zinc deficiency: its impact on human health and disease. *Adv Nutr* 2013;4(2):176–190. doi:10.3945/an.112.003210

34. Qu Z, Liu Q, Kong X, et al. A systematic study on zinc-related metabolism in breast cancer. *Nutrients*. 2023;15(7):1703. doi:10.3390/nu15071703

35. Costello LC, Franklin RB. Cytotoxic/tumor suppressor role of zinc for the treatment of cancer: an enigma and an opportunity. *Expert Rev Anticancer Ther.* 2012;12(1):121–128. doi:10.1586/era.11.190

36. Hashimoto R, Himoto T, Yamada M, et al. Antitumor effect of zinc acetate in hepatocellular carcinoma cell lines via the induction of apoptosis. *J NutrSci Vitaminol.* 2022;68(4):303–311. doi:10.3177/jnsv.68.303

37. Tang W, Liu H, Ooi TC, Rajab NF, Cao H, Sharif R. Zinc carnosine: frontiers advances of supplement for cancer therapy. *Biomed Pharmacother* 2022;151:113157. doi:10.1016/j.biopha.2022.113157

38. Chakraborti S, Chakraborty S, Saha S, et al. PEG-functionalized zinc oxide nanoparticles induce apoptosis in breast cancer cells through reactive oxygen species-dependent impairment of DNA damage repair enzyme NEIL2. *Free Radic Biol Med.* 2017;103:35–47. doi:10.1016/j.freeradbiomed.2016.11.048

39. Wiesmann N, Tremel W, Brieger J. Zinc oxide nanoparticles for therapeutic purposes in cancer medicine. *J Mat Chem B.* 2020;8(23):4973–4989. doi:10.1039/D0TB00739K

40. Banupriya SK, Kavithaa K, Poornima A, Sumathi S. Mechanistic study on thymoquinone conjugated ZnO nanoparticles mediated cytotoxicity and anticancer activity in triple-negative breast cancer cells. *Anti-Cancer Agents Med Chem.* 2022;22(2):313–327. doi:10.2174/1871520621666210412104731

41. Qi J, Zhang P, Zhang T, et al. Metal-doped carbon dots for biomedical applications: from design to implementation. *Heliyon.* 2024;10(11):e32133. doi:10.1016/j.heliyon.2024.e32133

42. Bhattacharya T, Preetam S, Mukherjee S, et al. Anticancer activity of quantum size carbon dots: opportunities and challenges. *Discover Nano.* 2024;19(1):122. doi:10.1186/s11671-024-04069-7

43. Ren J, Opoku H, Tang S, Edman L, Wang J. Carbon dots: a review with focus on sustainability. *Adv Sci* 2024;e2405472. doi:10.1002/advs.202405472

44. Benner D, Yadav P, Bhatia D. Red emitting carbon dots: surface modifications and bioapplications. *Nanoscale Adv.* 2023;5(17):4337–4353. doi:10.1039/D3NA00469D

45. Zheng B, Fan J, Chen B, et al. Rare-earth doping in nanostructured inorganic materials. *Chem Rev* 2022;122(6):5519–5603. doi:10.1021/acs.chemrev.1c00644

46. Xu -J-J, Lu Y-N, Tao -F-F, Liang P-F, Zhang P-A. ZnO nanoparticles modified by carbon quantum dots for the photocatalytic removal of synthetic pigment pollutants. *ACS Omega.* 2023;8(8):7845–7857. doi:10.1021/acsomega.2c07591

47. Khan F, Akhtar N, Jalal N, et al. Carbon-dot wrapped ZnO nanoparticle-based photoelectrochemical sensor for selective monitoring of H2O2 released from cancer cells. *Mikrochim Acta.* 2019;186(2):127. doi:10.1007/s00604-019-3227-x

48. Ostovar S, Pourmadadi M, Zaker MA. Co-biopolymer of chitosan/carboxymethyl cellulose hydrogel improved by zinc oxide and graphene quantum dots nanoparticles as pH-sensitive nanocomposite for quercetin delivery to brain cancer treatment. *Int J Biol Macromol.* 2023;253:127091. doi:10.1016/j.ijbiomac.2023.127091

49. Liang T, Feng Z, Zhang X, Li T, Yang T, Yu L. Research progress of calcium carbonate nanomaterials in cancer therapy: challenge and opportunity. *Front Bioeng Biotechnol.* 2023;11.

50. AkÇAn R, Aydogan HC, Mş Y, TaŞTekİN B, SaĞLam N. Nanotoxicity: a challenge for future medicine. *Turk J Med Sci.* 2020;50(4):1180–1196. doi:10.3906/sag-1912-209

51. Puspasari V, Ridhova A, Hermawan A, Amal MI, Khan MM. ZnO-based antimicrobial coatings for biomedical applications. *Bioprocess Biosyst Eng* 2022;45(9):1421–1445. doi:10.1007/s00449-022-02733-9

52. Wang GJ, Cai YP, Ma YJ, et al. Ultrastrong and stiff carbon nanotube/aluminum–copper nanocomposite via enhancing friction between carbon nanotubes. *Nano Lett.* 2019;19(9):6255–6262. doi:10.1021/acs.nanolett.9b02332

53. Sailer J, Nagel J, Akdogan B, et al. Deadly excess copper. *Redox Biol.* 2024;75:103256. doi:10.1016/j.redox.2024.103256

54. Morales M, Xue X. Targeting iron metabolism in cancer therapy. *Theranostics.* 2021;11(17):8412–8429. doi:10.7150/thno.59092

55. Li S, Ren J, Zhang W, et al. Glutathione and selenium nanoparticles have a synergistic protective effect during cryopreservation of bull semen. *Front Vet Sci.* 2023;10:1093274. doi:10.3389/fvets.2023.1093274

56. Dong S, Huang Y, Yan H, et al. Ternary heterostructure-driven photoinduced electron-hole separation enhanced oxidative stress for triple-negative breast cancer therapy. *J Nanobiotechnol.* 2024;22(1):240. doi:10.1186/s12951-024-02530-4

57. Yang B, Chen Y, Shi J. Reactive oxygen species (ROS)-based nanomedicine. *Chem Rev* 2019;119(8):4881–4985. doi:10.1021/acs.chemrev.8b00626

58. Wang M, Ren J, Liu Z, et al. Beneficial effect of selenium doped carbon quantum dots supplementation on the in vitro development competence of ovine oocytes. *Int J Nanomed.* 2022;17:2907–2924. doi:10.2147/IJN.S360000

59. Wang C, Wang B, Wei Y, et al. Effect of gentianella acuta (Michx.) Hulten against the arsenic-induced development hindrance of mouse oocytes. *Biometals.* 2024;37:1411–1430. doi:10.1007/s10534-024-00613-1

60. Ren J, Wang B, Li L, et al. Glutathione ameliorates the meiotic defects of copper exposed ovine oocytes via inhibiting the mitochondrial dysfunctions. *Ecotoxicol Environ Saf.* 2023;251:114530. doi:10.1016/j.ecoenv.2023.114530

61. Cruz-Gregorio A, Aranda-Rivera AK, Aparicio-Trejo OE, et al. GK-1 induces oxidative stress, mitochondrial dysfunction, decreased membrane potential, and impaired autophagy flux in a mouse model of breast cancer. *Antioxidants.* 2022;12(1):56. doi:10.3390/antiox12010056

62. Alsamri H, Al Dhaheri Y, Iratni R. Targeting triple-negative breast cancer by the phytopolyphenol carnosol: ROS-dependent mechanisms. *Antioxidants.* 2023;12(7):1349. doi:10.3390/antiox12071349

63. Wang S, Tian R, Zhang X, et al. Beyond photo: xdynamic therapies in fighting cancer. *Adv Mater* 2021;33(25):e2007488. doi:10.1002/adma.202007488

64. Yin X, Li Z, Lyu C, et al. Induced effect of zinc oxide nanoparticles on human acute myeloid leukemia cell apoptosis by regulating mitochondrial division. *IUBMB Life.* 2022;74(6):519–531. doi:10.1002/iub.2615

65. Ancona A, Dumontel B, Garino N, et al. Lipid-coated zinc oxide nanoparticles as innovative ROS-generators for photodynamic therapy in cancer cells. *Nanomaterials.* 2018;8(3):143. doi:10.3390/nano8030143

66. Chen H, Luo L, Fan S, Xiong Y, Ling Y, Peng S. Zinc oxide nanoparticles synthesized from *Aspergillus terreus* induces oxidative stress-mediated apoptosis through modulating apoptotic proteins in human cervical cancer HeLa cells. *J Pharm Pharmacol.* 2021;73(2):221–232. doi:10.1093/jpp/rgaa043

67. Ibrahim Abdel Aziz I, Riyad AA, Hussian AA, Mazen GM, Kannaiyan M. Solanum procumbens-derived zinc oxide nanoparticles suppress lung cancer in vitro through elevation of ROS. *Bioinorg Chem App.* 2022;2022(1):2724302. doi:10.1155/2022/2724302

68. Mishra P, Ali Ahmad MF, Al-Keridis LA, et al. Methotrexate-conjugated zinc oxide nanoparticles exert a substantially improved cytotoxic effect on lung cancer cells by inducing apoptosis. *Front Pharmacol*. 2023;14:1194578. doi:10.3389/fphar.2023.1194578

69. Mishra P, Ahmad A, Al-Keridis LA, et al. Doxorubicin-conjugated zinc oxide nanoparticles, biogenically synthesised using a fungus aspergillus niger, exhibit high therapeutic efficacy against lung cancer cells. *Molecules*. 2022;27(8):2590. doi:10.3390/molecules27082590

70. Motafeghi F, Mortazavi P, Shokrzadeh M. Anticancer activity of zinc oxide nanoparticles on prostate and colon cancer cell line. *Toxicol Res*. 2024;13(1):tfad127. doi:10.1093/toxres/tfad127

71. Berehu HM, Patnaik S. Biogenic zinc oxide nanoparticles synthesized from *Tinospora cordifolia* induce oxidative stress, mitochondrial damage and apoptosis in colorectal cancer. *Nanotheranostics*. 2024;8(3):312–329. doi:10.7150/ntno.84995

72. Li Z, Yin X, Lyu C, et al. Zinc oxide nanoparticles induce toxicity in diffuse large B-cell lymphoma cell line U2932 via activating PINK1/Parkin-mediated mitophagy. *Biomed Pharmacother* 2023;164:114988. doi:10.1016/j.biopha.2023.114988

73. Alhoqail WA, Alothaim AS, Suhail M, et al. Husk-like zinc oxide nanoparticles induce apoptosis through ROS generation in epidermoid carcinoma cells: effect of incubation period on sol-gel synthesis and anti-cancerous properties. *Biomedicines*. 2023;11(2):320. doi:10.3390/biomedicines11020320

74. George BP, Rajendran NK, Houreld NN, Abrahamse H. Rubus capped zinc oxide nanoparticles induce apoptosis in MCF-7 breast cancer cells. *Molecules*. 2022;27(20):6862. doi:10.3390/molecules27206862

75. Tang Q, Xia H, Liang W, Huo X, Wei X. Synthesis and characterization of zinc oxide nanoparticles from Morus nigra and its anticancer activity of AGS gastric cancer cells. *J Photochem Photobiol B Biol*. 2020;202:111698. doi:10.1016/j.jphotobiol.2019.111698

76. Kim Y-J, Perumalsamy H, Castro-Aceituno V, et al. Photoluminescent and self-assembled hyaluronic acid-zinc oxide-ginsenoside Rh2 nanoparticles and their potential caspase-9 apoptotic mechanism towards cancer cell lines. *Int J Nanomed*. 2019;14:8195–8208. doi:10.2147/IJN.S221328

77. Cheng J, Wang X, Qiu L, et al. Green synthesized zinc oxide nanoparticles regulates the apoptotic expression in bone cancer cells MG-63 cells. *J Photochem Photobiol B Biol*. 2020;202:111644. doi:10.1016/j.jphotobiol.2019.111644

78. Duan X, Liao Y, Liu T, et al. Zinc oxide nanoparticles synthesized from Cardiospermum halicacabum and its anticancer activity in human melanoma cells (A375) through the modulation of apoptosis pathway. *J Photochem Photobiol B Biol*. 2020;202:111718. doi:10.1016/j.jphotobiol.2019.111718

79. Li Z, Guo D, Yin X, et al. Zinc oxide nanoparticles induce human multiple myeloma cell death via reactive oxygen species and Cyt-C/Apaf-1/Caspase-9/Caspase-3 signaling pathway in vitro. *Biomed Pharmacother* 2020;122:109712. doi:10.1016/j.biopha.2019.109712

80. Ahamed M, Javed A, Kumar KM, Ahmad A. Zinc oxide nanoparticles selectively induce apoptosis in human cancer cells through reactive oxygen species. *Int j Nanomed*. 2012;7:845–857. doi:10.2147/IJN.S29129

81. Wang Y, Zhang Y, Guo Y, et al. Synthesis of zinc oxide nanoparticles from Marsdenia tenacissima inhibits the cell proliferation and induces apoptosis in laryngeal cancer cells (Hep-2). *J Photochem Photobiol B Biol*. 2019;201:111624. doi:10.1016/j.jphotobiol.2019.111624

82. Shi A, Liu L, Li S, Qi B. Natural products targeting the MAPK-signaling pathway in cancer: overview. *J Cancer Res Clin Oncol*. 2024;150(1):6. doi:10.1007/s00432-023-05572-7

83. Kciuk M, Gielecińska A, Budzinska A, Mojzych M, Kontek R. Metastasis and MAPK pathways. *Int J Mol Sci*. 2022;23(7):3847.

84. Zhang H, Cai L. Zinc homeostasis plays an important role in the prevention of obesity-induced cardiac inflammation, remodeling and dysfunction. *J Trace Elem Med Biol*. 2020;62:126615. doi:10.1016/j.jtemb.2020.126615

85. Wang Y, Zhao H, Liu Y, Nie X, Xing M. Zinc exerts its renal protection effect on arsenic-exposed common carp: a signaling network comprising Nrf2, NF-κB and MAPK pathways. *Fish Shellfish Immunol*. 2020;104:383–390. doi:10.1016/j.fsi.2020.06.031

86. Zhang Y, Wang H, Li J, et al. Peroxynitrite-induced neuronal apoptosis is mediated by intracellular zinc release and 12-lipoxygenase activation. *J Neurosci*. 2004;24(47):10616–10627. doi:10.1523/JNEUROSCI.2469-04.2004

87. Yu Y, Liu K, Wen Z, Liu W, Zhang L, Su J. Double-edged effects and mechanisms of Zn^{2+} microenvironments on osteogenic activity of BMSCs: osteogenic differentiation or apoptosis. *RSC Adv*. 2020;10(25):14915–14927.

88. Redman PT, Hartnett KA, Aras MA, Levitan ES, Aizenman E. Regulation of apoptotic potassium currents by coordinated zinc-dependent signalling. *J Physiol*. 2009;587(18):4393–4404. doi:10.1113/jphysiol.2009.176321

89. Rudolf E. Increased uptake of zinc in malignant cells is associated with enhanced activation of MAPK signalling and P53-dependent cell injury. *Acta Medica*. 2008;51(1):43–49. doi:10.14712/18059694.2017.7

90. Kaisman-Elbaz T, Sekler I, Fishman D, et al. Cell death induced by zinc and cadmium is mediated by clusterin in cultured mouse seminiferous tubules. *J Cell Physiol*. 2009;220(1):222–229. doi:10.1002/jcp.21754